



Stockholm
University

The antimicrobial effect of dermcidin investigated by
computational electrophysiology molecular
dynamics simulations

Björn Forsberg

Department of Biochemistry and Biophysics
Stockholm University

2013

Supervisor(s): Erik Lindahl (SU) / Bert de Groot (MPI-BPC)

Conducted in the group for biomolecular dynamics at the dept. of theoretical and computational biophysics, Max-Planck Institute for biophysical Chemistry, Göttingen, Germany

The barber put a hand on top of my head to turn me for a better look. Then he said to the guard, "Did you get your deer, Charles?"

I liked this barber. We weren't acquainted well enough to call each other by name, but when I came in for a haircut he knew me and knew I used to fish, so we'd talk fishing. I don't think he hunted, but he could talk on any subject and was a good listener. In this regard he was a good barber.

"Bill, it's a funny story. The damndest thing," the guard said. He removed the toothpick and laid it in the ashtray. He shook his head. "I did and yet I didn't. So yes and no to your question."

- Raymond Carver, *The Calm*

Contents

1	Popular science description	4
2	Abstract	5
3	Introduction	6
4	Introduction to the biological system under study	6
4.1	Cellular membranes	6
4.1.1	Lipids	6
4.1.2	Additional components	7
4.1.3	Bacterial membranes	7
4.2	AntiMicrobial Peptides (AMPs)and the antimicrobial effect	8
4.3	Human dermcidin	9
4.3.1	Prevalence and function	9
4.3.2	Structure	9
4.3.3	Membrane channel insertion pathway	10
4.3.4	Membrane specificity	10
4.3.5	Ion permeability	11
4.4	Aims	12
5	Introduction to the biophysical method(s) used	12
5.1	Molecular Dynamics	12
5.2	Parameters sets - force-fields	13
5.3	Simulations of membrane systems	14
5.4	Simulations of channels	14
6	Material & Method	15
6.1	Solution	15
6.2	Single membrane	15
6.3	Computational electrophysiology (CEP)	16
6.4	Simulations summary	17
6.5	Models	17
6.5.1	Ion-sidechain contacts	17
6.5.2	Channel radius profile	17
6.5.3	Ion conductance	18
6.5.4	Osmotic effect and solvation shell	19
7	Results	21
7.1	Bioinformatics	21
7.2	Structure stability	21
7.2.1	Solubility	21
7.2.2	Zn ion retention	22
7.2.3	Mutants	23
7.2.4	Truncations	23
7.3	Channel interior	23
7.4	Ion translocation pathway	25
7.5	Ion conductance	26
7.5.1	Voltage-dependence	26
7.5.2	Poissonian modeling	27
7.5.3	Water flux and conductance	27
7.6	Oligomerization and insertion pathway	28
7.7	Conclusions	29
8	Discussion	30
8.1	Results in view of previous work	30
8.2	Alternate interpretation	31
8.3	Outlook	31
8.3.1	Additional simulation	31
8.3.2	Experimental extension	32
8.4	Ethical considerations	33
9	Acknowledgments	33

Abbreviations

A_L	Area per Lipid
AMP	AntiMicrobial Peptide
aAMP	Cationic AntiMicrobial Peptide
cAMP	Anionic AntiMicrobial Peptide
C36	CHARMM36 parameter set
CEP	Computational ElectroPhysiology
CHARMM	Chemistry at HARvard Molecular Mechanics
COM	Center-of-mass
DFT	Density Functional Theory
GROMACS	GROningen MACHine for Chemical Simulations
HF	Hartree-Fock
HG	(lipid) Head Group
LPS	LipoPolySaccharide
LT	Lipid Tail
MD	Molecular Dynamics
PME	Particle Ewald Mesh (method for electrostatics)
QM	Quantum Mechanical
RMS(D)	Root Mean Square (Distance)
SDS	Sodium Dodecyl Sulfate
TMV	TransMembrane Voltage

1 Popular science description

The emergence of bacteria which are not affected by antibiotics has increased with their more extensive therapeutic use. This is known as antibiotic resistance, and because of it, there will exist an ever-present need to develop new and improved antibiotics. Peptides, which are essentially small proteins, can be produced by multicellular organisms and can additionally have properties which are antibiotic. What appears promising is that these types of antibiotics target a general property of almost all bacteria; their outer membrane. The way in which they do this varies among the types of peptides, but generally they break the membrane or allow small nutrients or ions to flow into or out of the bacteria, in a way which is lethal to them.

Dermcidin is a human such peptide which is secreted in sweat onto the skin, where it constitutes a part of the host immune defense. We endeavor to examine exactly how this human peptide antibiotic works to kill bacteria without harmful effect to native cells, on the basis of its reported structure. This structure implies the formation of a channel in the bacterial membrane, and we therefore direct our investigation to examine how such a channel could allow ions to flow across the bacterial membrane.

We use a method called molecular dynamics simulations, which takes a small part of a membrane and the surrounding environment (and the membrane channel), and computationally models how the different parts of the system behaves over time according to the physical laws of motion and the interactions they have with each other. This is immense work to calculate, and consequently we are limited to very small systems and very short simulation times. We are able, however, to get enough data to compare the results to experiments which also monitor the flow of ions across a membrane in the presence of dermcidin.

We find that computation and experiment are in agreement, and we are also able to explain why the channel only allows chloride ions to flow, and not sodium ions. Changing the channel structure, we are also able to improve the flow of ions, which could increase the effectiveness of a potential new antibiotic. In addition we are able to give hints of how the channel starts to get into the membrane, which is likely important for the specific targeting of bacteria, and not native cells.

2 Abstract

Eukaryotic organisms rely on several mechanisms to inhibit bacterial growth and infection, which mankind has sought to mimic to their specific and more targeted use. Due to the effect of adaptation by bacteria in response to new antibiotics, known as antibiotic resistance, there will be an ever-present need to develop new antibiotics to maintain their high efficiency. Peptide antibiotics appear to target a general property of the bacterial membrane, and should therefore constitute a mechanism which is highly robust to mutational adaptation. We employ a specialized implementation of molecular dynamics simulations to examine the membrane-interactions and -permeabilization caused by human dermcidin in bacterial membranes, which shows antibacterial properties in experiment and forms a transmembrane channel-like structure according to a solved crystal structure. We are able to conclude that charged sidechains maintain a structural rigidity of the oligomeric assembly which in turn enables it to maintain anion selectivity, and that lower oligomeric states constitute an potentially functional oligomeric precursor to the crystallized hexamer. Further we are able to improve channel conductance, and suggest experimental observables to corroborate the given conclusions. The knowledge gained forwards the knowledge-base needed to establish a categorization of the class of AntiMicrobial Peptides, and holds promise for further development as a possible broad-spectrum antibiotic.

3 Introduction

Bacteria are everywhere. This quickly becomes a problem for higher organisms, so many have evolved ways to limit bacterial growth, usually by producing *antibiotics*. Antibiotics or antimicrobials are drugs, molecules or molecular complexes that kill bacteria without becoming toxic to native cells, and are even used by bacteria themselves to limit foreign competition. But naturally in the course of evolution bacteria have come to know their enemies and in many cases responded to antibiotics by developing defenses. These defenses vary with the mechanism of the specific antibiotic, but are collectively said to constitute its *antibiotic resistance*.

The prevalence and increase of bacterial resistance to antibiotics constitutes an evolutionary mechanism that is unlikely to be circumvented by science due to the selective pressure the use of antibiotics exerts. The most immediate steps to ameliorate this resistance development is a drastic decrease in unnecessary prescription of antibiotics. Due to the finite lifetime of any antibiotic there is nonetheless a need to go beyond this and continually explore new such compounds for targeted use.

The common conception of antibiotics are small molecules or drugs which may target specific proteins in the bacteria, as was the case with the first antibiotics which became available in the 1930's and 40's. Another family of antibiotic compounds are short peptides, expressed in great variety throughout the range of eukaryotic organisms [1]. They are collectively known as antimicrobial peptides (AMPs). A great many of these AMPs display an amphipathic structure, which they commonly acquire upon interaction with biological membranes or membrane mimetics. This has led the investigations of their mechanisms to focus on their interactions with membranes, and their function within them. The principal improvement being that antibiotics based on interactions directly with bacterial membranes will be less sensitive to selective pressure, since they are each targeting a more general property of bacteria. Given a bacterial strain, it is in this view less likely that this bacteria would undergo such a fundamental restructuring of its genome or expression dynamics *in response to this antibiotic* so as to become resistant to it. It is this possibility which makes the research into AMPs important, not just because they would constitute a new antibiotic, but also one with a longer working lifetime.

The aim of this thesis is to explore the mechanism of one such AMP, human dermcidin [2], based on its structure and inferred function in a lipid bilayer. Like many AMPs, dermcidin shows a specificity for bacterial membranes, and usually this specificity is attributed to an affinity for a net negatively charged membrane, as most bacterial membranes incorporate negatively charged lipid head-groups and the LipoPolySaccharide (LPS). This is an intuitively convincing point for most AMPs, since the overwhelming amount of those known are net positively charged (cationic AMPs = cAMPs). There have been reports of increased resistance of bacterial strains to cAMPs, attributed to a change in lipid composition to a smaller fraction of negative headgroups [3], or inclusion of positively charged molecular constituents like D-alanylation of lipoteichoic acids in the outer membrane [4], but this is reportedly also equally due to factors other than a straightforward charge modifications, like an increase in membrane density [5]. Regardless there is reason to believe that human dermcidin behaves in an unorthodox way with regards to this, given its net anionic charge at neutral pH (anionic AMPs = aAMPs). This makes it an important contribution to the development of novel antibiotics.

4 Introduction to the biological system under study

4.1 Cellular membranes

4.1.1 Lipids

Lipids are the major constituents of biological membranes, providing a protective barrier for cytosolic processes, being highly dynamic and selectively semi-permeable. This cellular compartmentalization is essential for the efficacy of reactive mechanisms in a crowded cellular space [6], and the study membranes-associated mechanisms increasing importance.

The basic structure of a lipid is generally illustrated as a hydrophilic ball, from which emanates one or more hydrophobic tails, the most common being two. This reflects their general structure of a polar headgroup (HG) region and fatty acid (lipid) tails (LT). Collectively they form membranes by parallel stacking, forming two oppositely oriented amphipathic leaflets. In water hydrophobicity dictates these have their LT regions facing. While the composition of cellular membranes maintains a high plasticity and is subject to many regulating mechanisms, there are a number of frequently occurring lipid structures, termed 'standard' lipids. Standard lipids of a major class known as phospholipids, having a strongly polarized phosphate group in its HG region, are illustrated in a general schematic in Fig. 1.

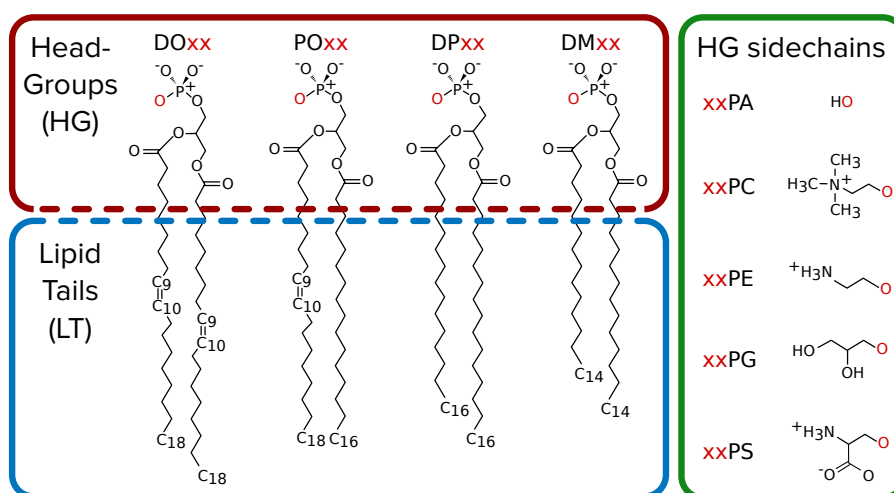


Figure 1: Standard lipids use in models of biological membranes represented by components. Note that all unsaturations are given at C9, whereas this position is a further degree of freedom in lipid structure which varies across species.

4.1.2 Additional components

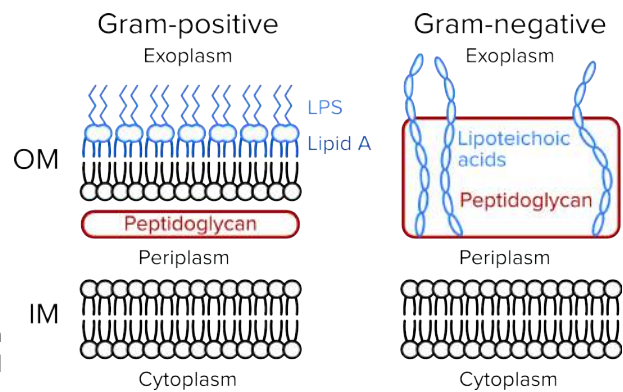
Membranes additionally contain many proteins that serve to regulate the selective transport of essential nutrients and other compounds through the membrane, as well as sensory detection and a host of other functions. Charge-rich molecules like proteins may affect the homogeneity, as will molecules like cholesterol, which affects the thickness and fluidity of the membrane. Proteins can also provide rigidity to some membranes, and together these factors paint a complicated picture, which might limit plasticity of the membrane and diffusion within it as compared to a (purely lipid membrane) idealization. We cannot hope to incorporate all these effects into a comprehensive synthetic system at present, particularly not by simulation studies, but will make the assumption that lipid properties determine much of the environment for proteins to interact with.

4.1.3 Bacterial membranes

Bacteria are usually classified as Gram-positive (G-pos) or negative (G-neg). This definition stems from their retention of a color dye, which interacts more dominantly with the membrane of G-Pos bacteria. This highlights that there are fundamental differences in membrane composition between the two classes. Whereas G-pos bacteria like *Staphylococcus aureus* (*S. aureus*) have a single bilayer and a thick (60nm) external peptidoglycan layer, G-neg bacteria like *Escherichia coli* (*E. coli*) have two bilayers separated by a periplasmic space which contains a much thinner (4nm) peptidoglycan layer (cf. Fig. 2). The two bilayers of G-neg bacteria are quite different in themselves, the outer incorporating the Lipid A as a base for lipopolysaccharides (LPS), which are known as *endotoxins* since these provoke immune responses in mammals. In G-pos bacteria there are similarly antigenic components, such as lipoteichoic acids.

	PE	PC	Negative	
			PG	CL
hepatocyte	23	39	18	1
erythrocyte	25	28	18	1
<i>S. aureus</i>	-	-	58	42
<i>Bacillus subtilis</i>	12	-	70	4
<i>E. coli</i>	80	-	15	-
<i>Pseudomonas aeruginosa</i>	60	-	21	11

Figure 2 & Table 1: Cytosolic membrane composition [7] of a human (eukaryotic) and representative bacterial (prokaryotic) Gram-positive and Gram negative cells



The lipid composition of bacterial membranes varies across species, and is largely very different from that of eukaryotic cells. To illustrate these differences, the bilayer composition of representatives of G-neg and G-pos bacteria are detailed in Tab. 1.

4.2 AntiMicrobial Peptides (AMPs) and the antimicrobial effect

Bacteria are frequently able to sustain a respiratory mechanism by establishing a proton gradient across their inner cytoplasmic membrane [8], utilizing it for energy synthesis. Its integrity is essential for the homeostasis and regulation of this and a number of other cellular functions beyond simple containment of cytosolic compounds. The targeting of such regulatory systems is the basis for many toxins in nature, which inhibit or stimulate these, disrupting normal function. While some antibiotics like penicillin inhibit proper cell-wall synthesis during cell division, many alter the nature of the semi-permeability of the membranes and cause depolarization, attributed to decoupling their transmembrane voltage (TMV) by ion gradient dissipation.

One such mechanism of depolarization is to provide facilitated diffusion, which in essence means that through

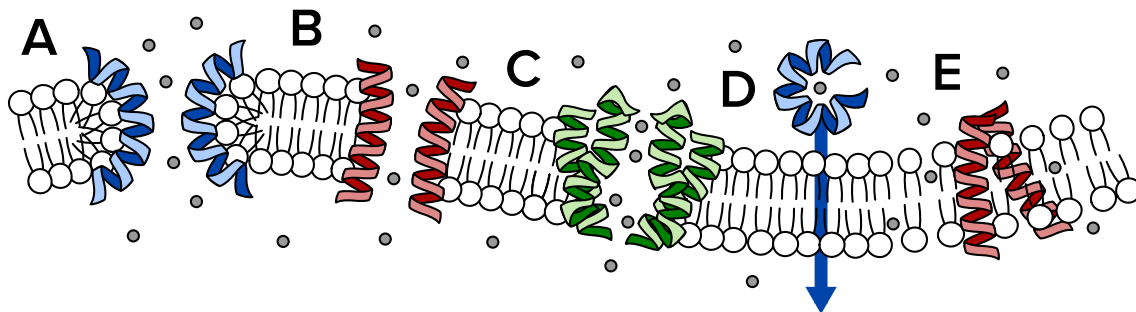


Figure 3: Commonly postulated modes of membrane-disruptive action by antimicrobial peptides. A) Toroidal pore. B) Barrel-stave pore. C) Channel. D) Facilitated diffusion. E) Carpet/Phase-perturbation.

binding it is enabled to cross the membrane. Valinomycin, an antibiotic commonly used to control cell growth in recombinant gene expression, acts in this manner by binding to K^+ ions. Mechanisms that are *pore-forming* describe molecules in the membrane aggregating to form a rigid structure that excludes lipids from a hollow center, forming a pore in the membrane. The prominent models that build on this idea are the barrel-stave and toroidal models, which mimic or curve the membrane, respectively. A similar but less radical destabilization of the membrane might also be sufficient to render cell division infeasible. Mechanisms that are *channel-forming* create a pathway across the membrane without disrupting the integrity of the membrane itself. Gramicidin is a notable example, common in medication against mild topical and mucosal infections, which forms a helix that spans the membrane and facilitates the selective conductance of monovalent cations such as K^+ and Na^+ , thereby depleting the transmembrane gradient.

4.3 Human dermcidin

4.3.1 Prevalence and function

Human dermcidin was first characterized by Schitteck and coworkers in 2001 [2] as an AMP which is constitutively expressed in eccrine sweat glands. Almost simultaneously, it was also found to act in the capacity of survival factor for neuronal cells during oxidative stress [9], and has in the last decade been systematically investigated in both of these respects [10–21]. Studies of DCD has found that its seemingly dual functions, as described above, are attributable to two distinct and separate precursor peptides.

The first is known as YDP-42, whose derivatives increase oxidative stress resilience in some types of neuronal

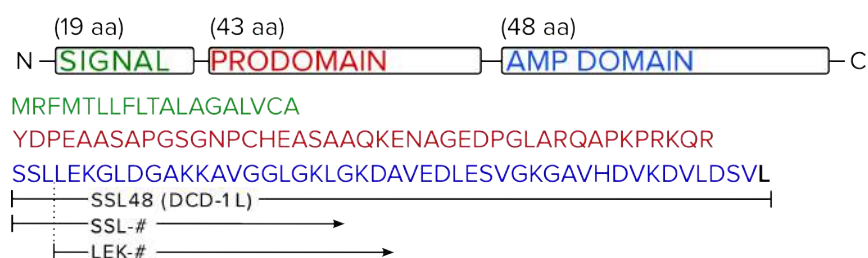


Figure 4: Functional components of the DCD gene, the signal peptide (green), the oxidative stress reducing peptide YDP-42 (red), and the antibiologically active AMP domain (blue). Figure adapted from an excellent review by Schitteck [19].

cells and are found to correlate to cachexia and skeletal muscle degradation in some cancer cell lines [10]. In the 110aa sequence of DCD, this peptide is localized to positions 20-62, and its derivatives are C-terminally cleaved versions of YPD-42.

The second precursor is DCD-1L, which is subject to post-translatory processing by proteases after being dispensed cutaneously through secretion [20], evident by the exclusive localization of DCD-derived AMPs to skin tissues. This is the precursor to a range of sequences found in human samples, which are found to have varying spectra of antibacterial effect [18]. These peptides are given to be named by their N-terminal triplet of residues followed by a number assigning their length. The full length precursor SSL48 (conventionally named DCD-1L) is found to exert antimicrobial action against both gram-positive and -negative bacteria below 100mg/l concentrations [16].

4.3.2 Structure

A structure of SSL48 in a 50%TFE (TriFluorEthanol) membrane mimetic was solved by NMR spectroscopy by Jung and coworkers in 2010 [11]. Their investigation showed a prominent transition from majorly coiled content in aqueous solution to helical in 50% TFE, which was even more significant in 20mM sodium dodecyl sulfate (SDS) micelles. The dominant helical regions were localized to residues near the C-terminus, with a notable flexibility centered around glycines 33 and 35. The N-terminal sequence is rich in glycines, which likely results in the lack of consistent helical secondary structure in this region. The flexibility due to these glycines has led to speculation of a channel-forming oligomeric structure where helical segments are aligned simultaneously perpendicular and parallel to the membrane surface [20]. A single oligomeric state has in deed been observed in samples of human sweat by way of native gel electrophoresis [23], but in this study there is no aggregation number assigned to this oligomeric state. Moreover this notion to some extent contradicts the observation of increased helical structure formation upon hydrophobic interface interaction [12].

A crystal structure of SSL48 has since been solved reveal a hexameric helix bundle with monomers aligned in anti-parallel, with a consequent 3-fold symmetry around its major axis. Due to this property it is invertible, that is, **it has no top or bottom with reference to the major axis**. This additionally means that each monomer is effectively experiencing the same interactions to its adjacent monomers, making each structurally identical. The length-wise offset of monomer helices is about 4 residues, allowing the C-termini to fold

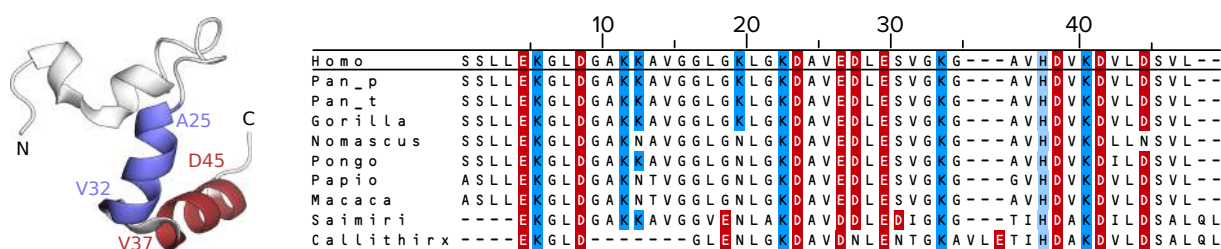


Figure 5: NMR-based structure assignment of SSL48 in 50% TFE [11] (pdb: 2KSG), and sequence alignment of AMP domain of DCD for available homologues under BLOSUM 10:0.2 scoring using ClustalW [22], alignment also highlighted by charged residues. The numbering of residues refers to the sequence of Homo Sapiens.

together to close of the ends of the oligomeric assembly, forming an interior of the oligomer of 2250 \AA^3 (cf. Fig. 6C).

Taking cylinders with two sides A and B along their length to represent typical amphiphilic helices, two such helices are likely to interact with similar sides facing, forming two distinct helix interfaces (A-to-A and B-to-B) when aggregated into higher oligomeric states. In the hexameric state of SSL48 we see anti-parallel matching consistent with this, the first interface (IF1) being highly polar and coordinating 2 Zn^{2+} ions, and the second (IF2) is almost exclusively hydrophobic, consisting of apolar residue sidechains (cf. Fig. 6A-B). The approximate 'locations' of these interfaces can be represented quite intuitively in a helical-wheel type plot as is illustrated in Fig. 6D-F. The coordination of Zn^{2+} ions in the active structure rationalizes the observed decrease of antibacterial activity of SSL48 when Zn^{2+} are absent. While a catalytic role of Zn^{2+} might still be feasible, this is discredited by the observation of decreased activity upon addition of the chelator EthyleneDiamineTetraacetic Acid (EDTA) to an active sample [20].

4.3.3 Membrane channel insertion pathway

In most models of action AMPs are required to insert into the lipid bilayer, forcing the question of how a secreted protein like SSL48 inserts into it. For proteins targeting non-native cells, a co-translational insertion pathway is not possible, but change of structure upon transition into a hydrophobic region can act to balance their solubility in polar solvents with that in a hydrophobic. A two-stage insertion model [24] is most plausible, given that as with many AMPs, CD-spectroscopy of SSL48 conclusively shows that helical structure is drastically increased upon interaction with model membranes [20]. But this does not conclusively establish the insertion pathway, which is possibly or even likely affecting the types of membranes that are susceptible, and by consequence its specificity and antibiotic spectrum.

4.3.4 Membrane specificity

The specificity of dermcidin and other AMPs for bacterial membranes is an essential property, showing broad spectrum activity that is specific to Gram positive and/or negative bacteria and a low but varying cytotoxic or hemolytic activity [20]. This is postulated to be principally linked to their affinity for the types of lipids and perhaps other constituents of their membranes [12] [13]. The generally accepted hypothesis relies on an electrostatic attraction due to net negative charge on bacterial membrane surfaces and the prevalence of AMPs that are cationic at neutral pH (cAMPs) [25]. Such a general interaction fulfills the principal criteria of broad-spectrum targeting, and offers a reasonable working hypothesis. Although strictly not a membrane selectivity mechanism, factors which further dictate insertion might none the less function as a means of specificity, critically dependent on the type of membrane, and by extension the function of that membrane (e.g. voltage gating etc.).

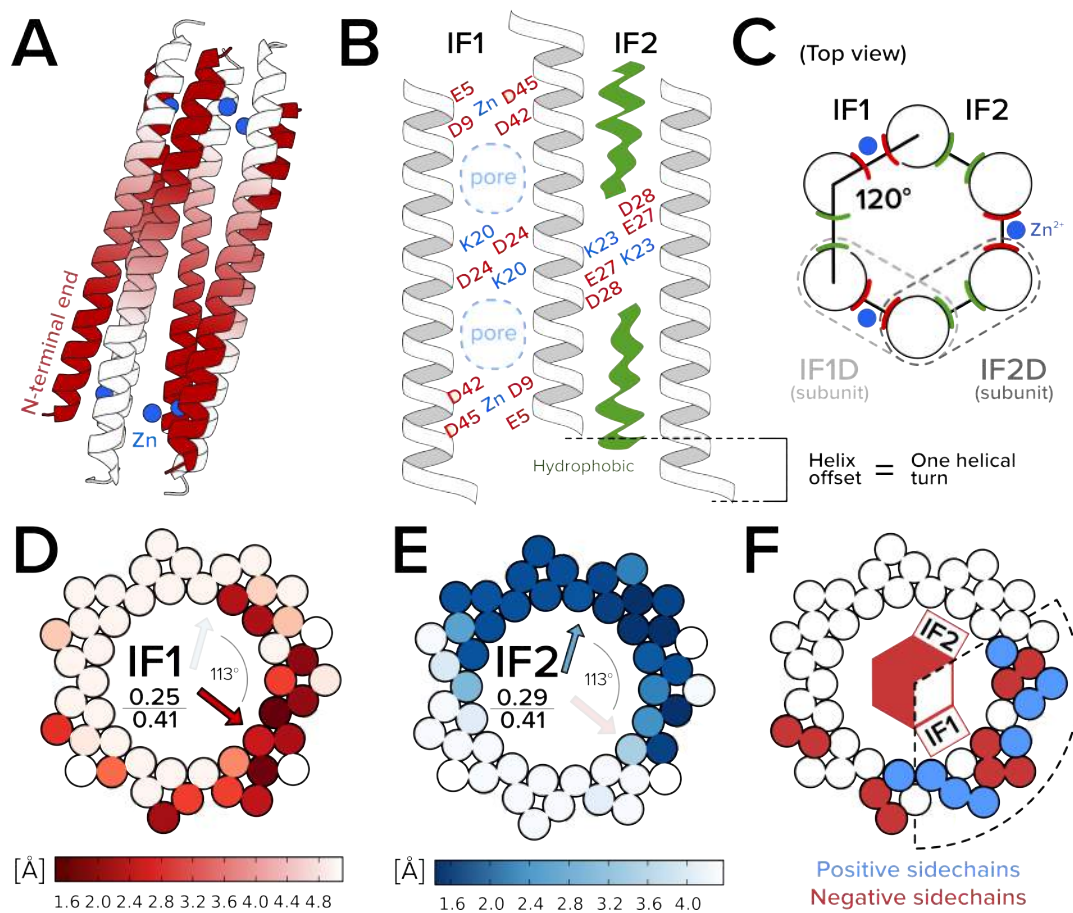


Figure 6: **A)** General structure of the anti-parallel SSL48 hexamer, colored by sequence orientation. **B)** The structural role of many ionizable residues rationalize a charge-zipper oligomer stabilization, predominantly across one of two monomer-monomer interfaces, which alternate around the six monomers, as further illustrated together with **C)** the dimeric subunit classification according to the nature of the monomer-monomer interaction. Interface locations in a helical wheel representation are established by weighting minimal distances of residues across the respective helix interfaces in **D)** and **E)** during simulation (for simulation details see sections 5.3-5.4). Given the minimum such observed distance the helical wheel idealization produces an expected optimal unanimity of direction, in both cases 0.41, and found in simulation as 0.25 and 0.29 respectively. Projected on a helical wheel plot, this rationalizes the **F)** hydrophobicity schematic of the SSL48 crystal structure helix.

4.3.5 Ion permeability

The resemblance of the SSL48 crystal structure to a TM helix bundle merited it to be investigated for its plausible activity as a membrane channel. Inserted in a model membrane molecular dynamics (MD; for details see section 4.1) system oriented normal to the membrane it acquires a 30° tilt (cf. Fig. 7B) attributed to the hydrophobic mismatch of the 6nm length of the oligomer to the 4nm membrane thickness. Linear permeation through the oligomer is prohibited by the offset C-termini restricting the interior cavity, and ion permeation instead largely occurs via entrance into (and exit from) 'pores' located in the polar interface IF1, resulting in a nonlinear 'S-shaped' permeation path (c.f Fig. 7C). A causal link between the tilt of the oligomer and permeation of ions through it is as of yet only speculative but far from unlikely, as this tilt affects the degree to which IF1 pores are exposed to solvent for diffusive access of ions. This also provides an appealing hypothesis for specificity by way of membrane thickness, at this point equally speculative.

In computational examination of SSL48 there is a clear selectivity for Cl^- ions over Na^+ ions, indicating its ability to depolarize some but not all ion gradients. Maintaining separate ion gradients across cytosolic membranes is often essential but requires proteins with an ability to exert selective control of those gradients. But the question begs to what end an AMP, intended to disturb function, should hold such a selectivity. This might again be linked to a specificity mechanism for bacterial membranes, since a decoupling of a certain

ion gradient could be lethal to one organism while only a slight perturbation to another. Effectively such a mechanism would target all biological membranes, but disturb a general function which is essential only to bacterial cells.

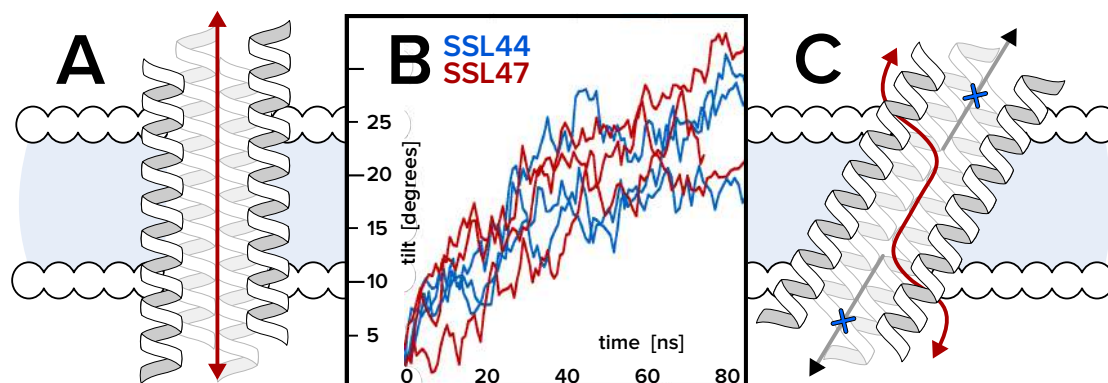


Figure 7: Illustration of the tilt of the crystal structure SSL48 hexamer observed when inserted in a model membrane during MD simulation. The canonical permeation path **A**) shows negligible activity, while the S-shaped permeation path **C**) contributes the major ion conduction.

4.4 Aims

To summarize, we offer a brief restatement of the questions pertaining to our study of SSL48 in explicit form:

1. Is there a structural basis for the observed anion selectivity, and is it significantly preserved across taxa?
2. Can an insertion pathway of dermcidin explain its selectivity for bacteria?
3. Is there a lipid-interaction basis for a localization selectivity of dermcidin to bacterial membranes?
4. Can we, using knowledge gained from answering the previous questions, enhance or modify channel function using rational design mutation(s) of the peptide sequence?

5 Introduction to the biophysical method(s) used

5.1 Molecular Dynamics

To describe the physical world we employ theory, which as far as is possible we describe analytically. The Schrödinger equation, in all its infamy, is the analytical center of Quantum Mechanics (QM), and describes how a system evolves with time at the most fundamental level. However in most cases where we attempt analytical models, these fail to be useful at some point. Either our assumptions run out of bounds and the model loses its grip on reality, or employing it becomes an infeasible effort compared to what we can get from it. Essentially, it's hard to solve the Schrödinger equation. The complexity of the formalism renders even simple systems feasible only through computational methods and to this end methods like Hartree-Fock (HF) and Density Functional Theory (DFT) were introduced. These reduce the complexity further by assuming for instance the Born-Oppenheimer approximation, which states that electrons respond faster and more readily to changes in external perturbations than the nuclei they surround, treating the latter as essentially fixed charges. DFT for instance, reduces the quantum mechanical description of those electrons from a distribution of *probability* around atomic nuclei, to a charge *density*. It is still a relatively expensive computational method, only able to describe systems of the order of 10^2 atoms to any efficient degree at present [26]. To increase the size of the system we thus need to further reduce the complexity of the system, beyond the numerical treatment of QM.

Molecular Dynamics (MD) software makes this reduction by assuming that atoms behave according to the classical Newtonian equations of motion, governed by idealized interaction models with empirical parameters. In simple terms, this means that the nucleus and electrons of each atom is made into a single particle, and that the motion of this particle behaves according to classical physics. Its motion is then numerically treated by the sum of force contributions from simple models of interaction with its neighboring particles, as depicted in table 8. These terms describe different aspects of atomic interactions, and taken together it becomes a still less accurate, but wholly more efficient scheme to study molecular phenomena several orders of magnitude larger than what QM methods are able to, both in terms of system size and timescale. But MD means leaving quantum mechanics behind, and the treatment of bond rearrangements as it occurs in chemical reactions is in general not possible. There *are* methods to appreciate differences between different chemical structures by using MD, but these are artificial methods not usually reproducing the kinetics or chemistry of the reaction itself.

Interaction	Model	Fit
Bonds	Harmonic	IR
Angles	Harmonic	IR
Dihedral	Bradley-Urey	QM
Pauli rep. & Dispersion	Len.-Jones	TD
Electrostatic	Coulomb	QM

$$V_{\text{ff}} = \sum_{\text{bonds } i} V_b^i + \sum_{\text{angles } j} V_a^j + \sum_{\text{impropers } k} V_g^k + \sum_{\text{dihedrals } l} V_{\text{dh}}^l + \sum_{\text{pairs } m,n} \left(V_{\text{Coul}}^{m,n} + V_{\text{LJ}}^{m,n} \right)$$

Figure 8 & Table 2: Description of MD interaction potentials used in C36, picture adapted with kind permission of Prof. H. Grubmüller.

5.2 Parameters sets - force-fields

In MD one utilizes so-called force-fields, which are nothing more than the constants that characterize the different interactions listed in Fig. 8. These force-field parameters have been determined from fitting to molecular properties observed, like boiling points, solvation free energies or secondary structure formation. It thus replaces the QM description with an empirical model that reproduces molecular phenomena accurately, a so called molecular mechanical (MM) model. Which phenomena is best reproduced and has the highest predictive value depends of the choice of fitting data used when constructing a certain force-field, and a number of FFs have been established using different methods and data with more or less specific areas of application in mind. The validity of a force-field is also critically judged by accurate reproduction of the same type of observable thermodynamic properties.

The parameter set CHARMM36 (C36) was introduced in 2010 to address a number of discrepancies in the back-calculated experimental observables of lipid bilayers. Majorly there was concern about the area per lipid (A_L), which in experiment were in the 60-65 Å² range, but were consistently underestimated by up to 15% [27]. Significant corrections were increases in atomic partial charges and LJ-interaction potential parameters in the HG region, which as a consequence increased polarity and solvation of the HGs themselves, which is attributed to a drastic correction in A_L . Reportedly lipid bilayers may in C36 be simulated under NPT ensemble for standard lipids, although caution should be exercised concerning unsaturated lipids, such as DOxx and POxx (cf. Fig 1), where C36 constitutes a lesser improvement. Lipid parameters were established

and evaluated based on pure lipid bilayers, which constitutes another possible caveat in simulating a mixed lipid bilayers.

5.3 Simulations of membrane systems

The fundamental property of lipid bilayers is their phase. Lipids self-assemble into bilayers (lamellar phase) under certain circumstances, as was reproduced by simulations early on in the computational studies of lipids [28]. While lipids can form other structures under different conditions, such as micellar or hexagonal phases, there are within the lamellar phase a continuous spectra of fluidity, which is often discretized into a gel and liquid crystalline phase [29]. The former is characterized by a low lateral diffusion of lipid molecules and a higher degree of ordering of the LT region, resulting in a stiffer and thicker bilayer. The latter is more dynamic and as implied 'fluid', enabling a more dynamic behavior as is essentially employed in most biological systems. The variables that serve to control the transition along this reaction coordinate are many, such as temperature, bilayer and solvent composition and so forth. Moreover, the electrostatic description and pressure coupling used in simulations affect the packing of lipid HGs and thus the A_L , introducing further computational considerations. A challenge in utilizing simulations in the study of membranes is therefore to continually legitimize the bilayer phase behavior in view of observables like lateral diffusion and A_L . The electrostatic description is tuned according to the forcefield and components, while the pressure coupling is implemented semi-isotropically if need be, in order to maintain A_L . This method is frequently utilized by way of assuming a joint causal relationship between phase behavior and the observable A_L , and is known as an NP_aT-(or NPAT-)ensemble. In addition a temperature slightly higher than biologically relevant may be used to avoid the gel phase.

One way to ameliorate the cost of simulating full lipid bilayer systems explicitly is to utilize a united-atom description of the lipid components, meaning the exclusion of explicit hydrogen. For a single lipid molecule this signifies a reduction from some 130 atoms to about 40, affecting mainly the hydrophobic LT region and without dramatic loss of accuracy in its description [30]. Further representing the lipid bilayer as a continuous region with known dielectric properties enable even more efficient simulation. The immediate drawback to such methods are similar to implicit solvent methods, in that while statistical error from sampling is reduced (since one is inherently using average properties to describe the bilayer) there is no way to correctly estimate the entropic part of the free energy difference between examined systems that the discretization of lipids would contribute [31]. Observables that legitimize the membrane description such as A_L and lateral diffusion rates also become unattainable.

However with increasing computational power, implicit solvation of explicit lipid bilayers have enabled the macroscopic observations of lipid bilayers to be examined using coarse-grained or even atomistic simulations. Vesicle fusion, membrane rupture and induced curvature are a few properties that have been studied, and is continually improving the description of lipid bilayers that is available to computational biology. United-atom and all-atom simulations of membranes are today a common tool to improve drug screening, which often target proteins which oligomerize in a lipid bilayer or regulate a selective permeability of the same membranes. The cost of using explicit components is naturally weighed against the required detail of the sought observables, wherein the bilayer may or may not constitute a structurally active role, often limiting the necessity of its explicit description beyond that of providing a specific lamellar hydrophobic phase.

5.4 Simulations of channels

Computer-based investigations of membrane proteins have flourished in recent decades due mainly to the high level of detailed knowledge they provide. Experimental studies still most commonly provide structures and functional context, but with the advance of programs and tools used by computational biology, their complementary use to identify and verify functional modes has increased. Initial investigations were limited to studying the interactions of protein structures with lipid bilayers to study structural transitions, being relatively

inexpensive simulations that did not require long timescales or high number of particles required.

The kinetic information of how permeation through protein channels is regulated is a fruitful end of a method with atomistic detail, and MD is routinely able to address such phenomena. Channels have been identified where internal motion in the protein has been found to open or close the channel, which in some cases can be observed in simulation and thereby further characterized [32]. Simulations have also been able to provide details of selectivity for certain permeants in channels, one of the most important features of membranes channels. The channel interior of Aquaporins have been shown to orient water molecules to prohibit proton diffusion according to the Grotthus mechanism [33], thus avoiding the dissipation of a sustained pH gradient. A selectivity mechanism of potassium channels has been shown to exclude other monovalent ions, and is presently under investigation, principally by MD, in order to determine the causality in its selectivity filter [34]. For simulations to replicate the flux of some permeant across a membrane, one needs a physically realistic driving force, and in order to observe frequent enough permeation events in simulation to attain statistical certainty this driving force is often exaggerated for increased sampling. This driving force may be electric potential, chemical potential or otherwise, but should be quantifiably imposed on the system. The most common method is to impose a force on the particles of a simulation in accordance with an external voltage. This method has limitations concerning physical justification and quantification, as periodic boundaries normal to the applied field make the calculation of the applied TMV impossible due to the effective short-circuiting of the bulk regions. The permeation behavior across channels can however be legitimized since this is often far from the periodic boundary, and the magnitude of the voltage claimed through the magnitude of force acting on charges particles. The inability to calculate the existing potential however limits this claim, as the potential cannot be said to be well-defined.

MD and its computational detail thus directs itself to explain the details of protein dynamics which one is hard pressed to resolve using other methods. It is also in this aspect we utilize this method presently, where experiment has made an observation without sufficient evidence of mode of action or functional knowledge. We use MD in order to explain how specific interactions dictate the function of SSL48.

6 Material & Method

The MD protocol in this thesis was implemented using the GROningen MAchine for Chemical Simulations (GROMACS) software package, version 4.5.5-4.6 [35] and tools under the CHARMM36 (C36) parameter set (force-field) [27]. In all simulations which were used for data analysis default protonation states were used. (Positive sidechains: Arg, Lys, His / Negative sidechains: Asp, Glu).

6.1 Solution

Solution simulations were constructed by solvation of protein structure in 150mM NaCl, followed by energy minimization. Thereafter followed Short (50 ps) NVT- and NPT ensemble equilibrations. Production simulations were then run and initial phase not used for analysis on the grounds of potential ongoing equilibration. A 2 fs integration time-step was used, along with a coulomb radius of 1.0 nm and VdW cutoff, under treatment of the Particle Ewald-Mesh (PME) electrostatics. Temperature coupling was made to 298K with a $\tau_t = 0.1\text{ps}$ using V-rescale to treat the protein and non-protein atoms separately. Parinello-Rahman (PR) pressure coupling was implemented to 1 bar, using $\tau_p = 2.0\text{ps}$. The number of water molecules was on the order of $3 \cdot 10^4$, and the cubic box dimension 9.9 nm.

6.2 Single membrane

Lipid bilayer patches were acquired from the web-based interface CHARMM-GUI [36], and consisted of 72 POPE and 24 POPG molecules in each lipid leaflet, giving a total of 192 lipids at a 3:1 mixture of negative HGs in a lipid bilayer patch. To set up patches, these were solvated in 150mM NaCl using an increased

carbon VdW-radius of 0.45\AA (default 0.15\AA), to the effect of excluding water or ions to be inserted in the membrane hydrophobic region. This also excludes some space around the HG region, which is rectified by a short (ps-range) double precision equilibration without pressure coupling and restored carbon VdW radius. The hydrophobic regions of the two leaflets separate during this equilibration in order to fill the excluded HG region, but this is in turn quickly corrected during further NPT-equilibration.

The protein structure was inserted into patches using `g_membed` [37]. The net system charge was then neutralized by the addition of Na^+ ions to compensate introduced HG charge. A 2 fs integration time-step was used, along with a coulomb radius of 1.3nm, VdW switch of 0.8nm and VdW-radius of 1.2nm, under treatment of PME. Temperature coupling was to 310K with a $\tau_t = 0.1\text{ps}$ using the V-rescale, coupling the protein, non-protein, and lipid atoms separately. Berendsen pressure coupling was implemented to achieve NPaT-ensemble, with $\tau_p = 1.0\text{ps}$. VdW and Coulomb potential shift modifiers were used. The number of water molecules was on the order of $1.5 \cdot 10^4$, and box dimensions $7.6 \times 7.6 \times 11.3$ nm. For additional trajectories, either complete iteration of the construction protocol, or varying velocity generation seeds for equilibrations were used.

6.3 Computational electrophysiology (CEP)

To exert a force upon ions that closely mimics a physiological transmembrane voltage (TMV) we utilize computational electrophysiology (CEP), a dynamical protocol implemented in GROMACS by Carsten Kutzner and coworkers [38] which maintains a set stoichiometry of any choice of molecules between two compartments of a simulation unit cell. This requires the extension of the simulation to include two (2) membranes in order to maintain periodic boundaries in all spatial dimensions. Excess molecules detected in either compartment are switched for a water molecule in the other, thereby maintaining the set imbalance. The methodology is summarized in figure 9.

Unless otherwise stated, the maintained ion imbalance is set to 7 cations, achieving a 14 cation difference

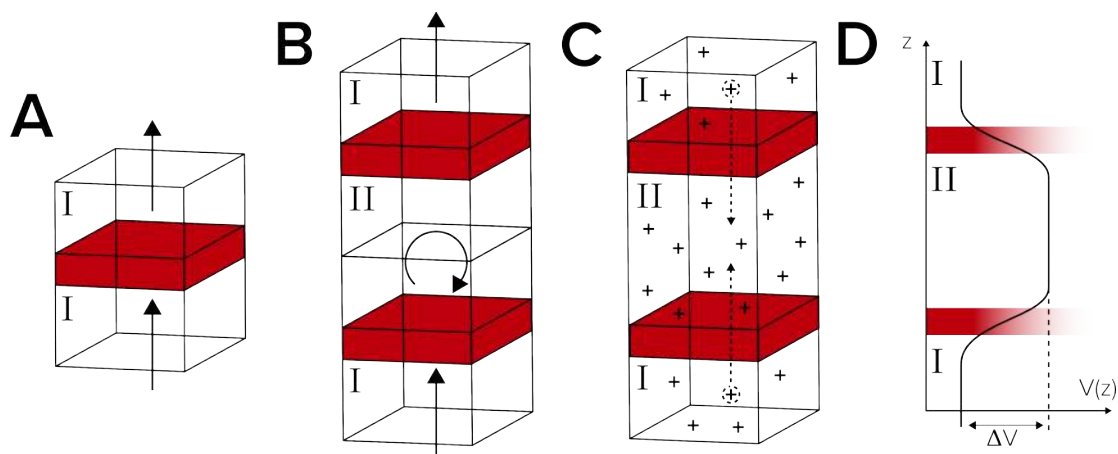


Figure 9: Schematic illustration of computational electrophysiology extension of simulation box. A single membrane allows a single compartment using complete periodic boundaries (A). Doubling the system creates two separate compartments I and II (B), which can be used to establish an electrochemical imbalance (C), which leads to a transmembrane voltage (D), dependent on gradients magnitude and box dimensions.

between compartments. The resulting voltage is both variable with the box dimensions and stochastically due to ion diffusive movement, but is generally in the 0.1-1V range in our simulations (cf. Fig. 20). Virtual sites were in some cases used on protein and lipids, to allow a 4 fs integration time-step. NPaT ensemble was then implemented to assure legitimacy of lipid thermodynamic properties. No VdW or Coulomb modifiers were used in CEP setups.

6.4 Simulations summary

The MD simulation trajectories that the following results are based upon are listed below. For further details consult method description.

	Structure	Solution	Membrane	CEP
WT	SSL48	$\times 3_{(150)}$	$\times 3_{(400)} \dagger$	$\times 3_{(200)} \ddagger$
Mutants	K20N	$\times 1_{(125)}$	-	$\times 3_{(200)} \ddagger$
	K23SE27S	$\times 1_{(125)}$	-	$\times 3_{(200)} \ddagger$
Dimers	IF1D	$\times 1_{(360)}$	$\times 3_{(200)}$	$\times 3_{(75)} \S$
	IF2D	$\times 1_{(290)}$	$\times 3_{(200)}$	$\times 3_{(200)} \S$
Truncations	SSL44		$\times 3_{(100)}$	$\times 3_{(200)}$
	SSL47		$\times 3_{(100)}$	$\times 3_{(200)}$
Osmotics	AQP1	-	-	$\times 2_{(100)} \P$
	SSL48	-	-	$\times 2_{(140)} \P$

Table 3: How many trajectories were carried out, indexed is the approximate duration of each in ns. (\dagger = vsites on protein, \ddagger = vsites on protein and lipids under NPaT, \S = NPaT, \P = no TMV)

6.5 Models

6.5.1 Ion-sidechain contacts

The interaction of ions with residue sidechains during permeation is a principal point of analysis, and we evaluate this dynamical property by how frequent and persistent a close distance between ions and protein components is maintained. The discrimination of a contact is set by a hard cutoff at 3.5Å, representing a distance that for both sodium and chloride incorporates their first solvation shell (cf. Fig. 18). While interaction with residue sidechains may differ in average length compared to that with a water molecule, this still symbolizes the desolvation of the ion to form the contact, and is thereby a justified measure of interactive distance.

6.5.2 Channel radius profile

We examine local steric restrictions during ion permeation and the integrity of the channel interior using the program HOLE [39] [40]. We establish a time-averaged mean radius resolved along the channel axis, and the associated fluctuation as the standard deviation of the determined radius at a given coordinate along the channel. This fluctuation might however be skewed, and not well-represented by a symmetric Gaussian. Certainly at points where the value of the fluctuation approaches that of the radius this distribution must indeed be skewed. At each position along the examined axis the distribution of residue(s) constituting the restriction at that position is also found. As HOLE uses a Monte-Carlo (MC) algorithm to find the optimized position *and* maximized radius of a circle in a plane normal to the axis, there is effectively three residues constituting this restriction. However due to numerical inaccuracies one is given as the closest to the optimized circle position, and this defines the restriction. Under the assumption that the numeric inaccuracies cancel out in the limit of a large number of simulation frames, this does not compromise the consistency of results.

The non-linear permeation path observed for this channel structure (cf. Fig. 10) makes a complete path analysis elusive using HOLE, but is sufficient to examine the central cavity of the protein satisfactorily. Fig 10 illustrates the range across which the channel radius is determined and the general procedure the program HOLE uses to establish the radius. The protocol iterates over MC planes to establish a channel profile for each frame of a simulation, which is then averaged over entire simulations.

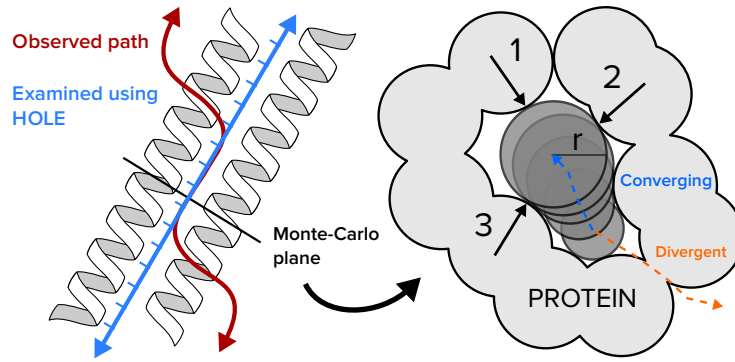


Figure 10: Schematic illustration of channel radius determination range, procedure and MC algorithm. The observed permeation path for ions does not follow the canonical, linear path but rather a S-shaped curve (red), inaccessible by direct analysis. The MC algorithm does not guarantee convergence, but occasional divergence produces only minimal artifacts in results.

6.5.3 Ion conductance

Assuming that the current of ions is dependent on the externally applied voltage, we use basic electrical laws to establish the conductance of ions as a property which determined under assumptions of ideal conditions follows a linear voltage dependence to yield a measure (1) that is independent of the applied TMV. We use two separate methods to quantify conductive behavior, both relying on this simple relation for conductance as the quota of current to voltage:

$$G = \Omega^{-1} = I/V \quad (1)$$

1. Non-redundant bootstrap counting of ion permeation events

To generate a reliable fluctuation measure and increase the confidence in TMV magnitude to ion current, i.e. conductance, the TMV and corresponding current are determined as averages over 50ns windows, spanning entire simulations. These several values of ion conductance can be used to assess the voltage-current correlation in addition to establishing the overall average.

2. Poisson process modeling

If permeation events are stochastic events, they occur according to a general Poissionian process, like that of radioactive decay observations. The distribution of interarrivaltimes between subsequent permeation events is in this view an exponential distribution $\lambda e^{-\lambda t}$, and given multiple *independent* such processes their individual rates are additive, that is;

$$\sum_i \lambda_i = \lambda_{tot} \quad (2)$$

This establishes a credible metric for the independent permeation by different ion species. However a lack of evidence for such an independence cannot be claimed any more than a breakdown of *either* assumption (Poissonian/independent). Formally we establish the measure Δ_λ :

$$\Delta_\lambda = \lambda_{ion} - \lambda_{Na} - \lambda_{Cl} \quad (3)$$

(where λ_{ion} is the rate for permeation of any ion) and judge the deviation of Δ_λ from 0. The confidence the observed independence is assessed by means of artificially replicating the distribution of Δ_λ from the observed number of permeation events f across the total simulation time. Effectively one iteratively recreates the observed permeation numbers, knowing that the processes are indeed independent, and judge the probability to none the less interpret the observed value of Δ_λ as dependent.

The correlation of permeating ions has been observed in computational studies of nanoscale pores [41], and is a viable tool to classify the permeation dynamics, and their casual relationship. This also augments the

analysis of conductance to assess whether the distribution of events is consistent with the average behavior, i.e. if we can consider the process as an uninterrupted stochastic process, which would indicate it is limited by diffusive factors rather than some energetic barrier. A discrepancy between the above stated measures 1. and 2. may additionally separate average behavior from conductive capacity.

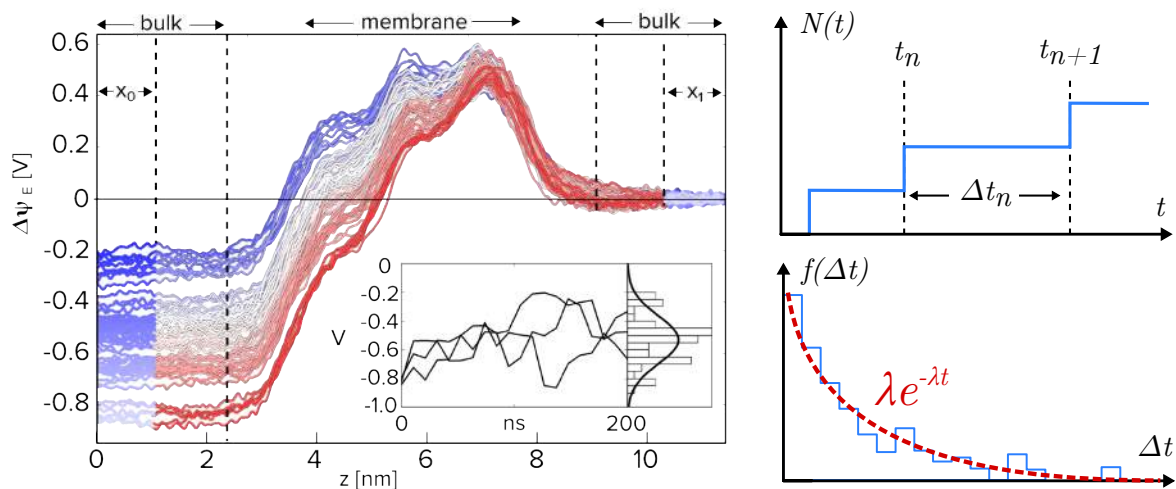


Figure 11: Determination of TMV using reference bulk regions x_0 and x_1 (only half a simulation box shown), colored by total voltage drop, inset describing the time evolution of three 200ns simulations. Ion permeation is analyzed according to interarrival times Δt , the distribution of which yields a rate parameter for the Poisson-type process of observing permeation events.

6.5.4 Osmotic effect and solvation shell

Ion flux through a hydrated membrane pore will to some extent have a positive correlation with water flux due to the presence of a full or partial hydration shell around ions, and water conductance therefore becomes a quantifiable effect. In using CEP, restraining the motion of membranes normal to their surface approximately maintains the water volume of both compartments, which for highly conductive channels is necessary unless one compartment should be depleted of water. As CEP maintains a fixed difference between compartments such a volumetric perturbation would shift the ion concentration towards the water-depleted compartment, possibly affecting the ratio of conductance by introducing a chemical potential difference. This *would* be countered by an osmotic effect, but this is partly much too slow to fully compensate this effect [41], and given that ions are used to neutralize the overall system charge, an osmotic pressure is not necessarily opposite to ion flow. Calculated for two channels, the experimental conductance 81 pS of SSL48 under extremum voltage of 1.0V, one finds an upper bound of 1.0-1.2 ions/ns, which at full (6 molecules) solvation gives a potential water flux of 600-700 water molecules over a 100ns trajectory. This is judged tolerable compared to the $1.5 \cdot 10^4$ water molecules in each compartment of our simulations, therefore not mandating bilayer position restraints.

However, to still quantifiably verify that no osmotic or otherwise driven waterflow persists in our simulations apart from this, we construct control simulations using CEP with a concentration gradient but no charge imbalance, producing no net TMV.

Implemented over longer timescales (μ s-range) there has been reports of consistently occurring time-dependent decrease in conductance using CEP, perhaps attributable to either the hydrobaric or chemiosmotic forces we introduce by restraining the bilayers or not, either of which would introduce a systematic and cumulative error. Consequently, several shorter trajectories appear the immediate remedy for statistical assurance of conductance determination. Voltage fluctuation however appear to limit the accuracy of voltage determination to the 10^1 ns range, preferably going into the 10^2 ns range.

We also inspect the solvation number, i.e. the number of water molecules energetically associated with ions

during permeation, from a histogram of the number of water oxygens within 3.5\AA of each ion, resolved along the membrane normal axis. Such an analysis may also reveal significant and/or localized desolvation. Given credible evidence for the independent permeation pathways for each ion species as described in section 5.5.3, we may treat a net flow due to independent and opposite ion currents under the assumption of similar solvation shells. Thus the net current of ions j_{Na} and j_{Cl} should under this assumption correlate with the net water flow, and we may establish an effective solvation shell during permeation, signifying the number of water molecules that accompany the ion during permeation.

$$(j_{\text{Na}} + j_{\text{Cl}}) \cdot (N_s - 1) = \Delta N_{\text{H}_2\text{O}} \quad (4)$$

In (4), the subtraction of 1 to the solvation number N_s accounts for the switching protocol we implement, in which we create an artificial water transport identical to the net ion flux. Using this relation we may determine N_s for any set of values for which we know the ion currents, and acquire a water conductance analogous to that of ion permeation.

To deconvolute the possible influence of osmotic effect in simulation form the net water transport due

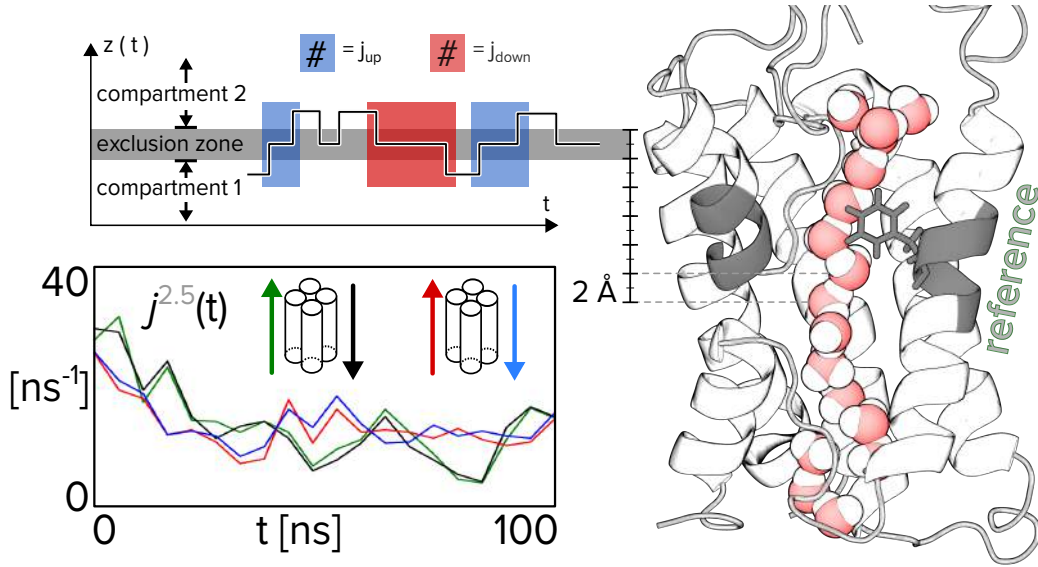


Figure 12: The reference regions of the AQP1 monomer unit is used to establish the center coordinate for the exclusion zone, which separates the compartments. The choice of thickness of this exclusion zone determines the magnitude of the fluctuation to be registered as a current, as directional flow across it is counted as forward and backward rates, respectively.

to ion flux further, control simulations were used to quantify the possible effect. Under more drastic ion concentration gradients we use the water channel aquaporin-1 (AQP1; pdb-code 1J4N) to attain a semi-permeable membrane excluding ion permeation. The movement of one water molecule in the single-file water column of aquaporins, across a distance equal to the spacing between water molecules in this same column, constitutes the net transport of the entire column, and thus a permeation event. This enable us to examine backwards and forward rates across the compartments, the method is illustrated in Fig. 12. The water flux was analyzed under the assumption of a purely entropic driving force, using the linear dependence [42]

$$j = p_f \cdot \Delta C \quad (5)$$

on concentration difference. To determine whether a possible discrepancy from the linear relation (5) due to *i)* the breakdown of the description of the entropic contribution to the osmotic force, or *ii)* the contribution of a significant physical driving force apart from the entropical one, we examine whether the exchange rates between compartments were consistent with a population (concentration) probability. This constitutes a

necessary but not sufficient requirement to accept *i*) in favor of *ii*).

7 Results

7.1 Bioinformatics

A projection of the SSL48 sequence onto a helical wheel plot indicates polar/charged residues are concentrated to an $\approx 120^\circ$ circular section (cf. fig 13), 17 out of 48 residues being ionizable (35%) and 4 additionally polar (9%). A 120° region indicates a three-fold symmetry in plausible oligomeric assemblies. Adjacently anti-parallel helices results in two separate interfaces necessarily separated by 120° in a helical wheel representation, and also prohibits oligomers with odd aggregation numbers. A three-fold symmetry thus rationalizes the hexameric state as the lowest oligomer. Interfaces are characterized (cf. Fig. 13) as predominantly hydrophilic (IF1) and hydrophobic (IF2), perhaps implying preferential oligomerization in solvent and membrane respectively. Most importantly though, the localization of the interfaces enables a schematic characterization of the hexamer (cf. Fig. 13B) that realizes a minimization of polar exterior, consistent with a hydrophobic phase localization, rather than the solvent crystallization environment.

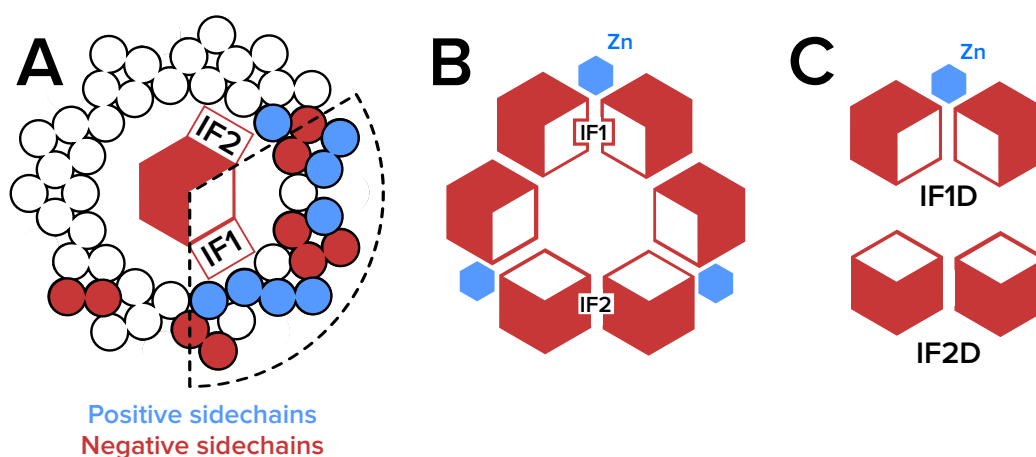


Figure 13: When considered in a **A**) helical wheel representation a 120° region of polar residues is identified, and under dynamic analysis two separate interfaces to neighboring helices are observed, IF1 and IF2. This rationalizes a **B**) schematic top view of the oligomer structure that maintains a polar interior and hydrophobic exterior. Moreover it highlights the distinct dissimilarity of the plausible dimeric structures **C**), named according to their interface interactions.

7.2 Structure stability

7.2.1 Solubility

While the hexameric structure is argued as native to the membrane by its minimized polar exterior, its polar interior is still solvated in solution, leaving little driving force for a hydrophobic collapse. This affords stability in solution and simultaneous preferential membrane insertion, confirmed by clear stabilization upon insertion (cf. Fig. 14 and Tab. 4). Stabilization of the hexamer *does* appear countered by introducing a TMV, indicating more frequent competitive interactions of solvent with mid-sequence residues, the hydrophobic environment apparently stabilizing the inserted oligomer by solvent exclusion. In solution IF1 maintains a normal distributed helix-helix center-of-mass (COM) distance of $1.33 \pm 0.05 \text{ nm}$. The hydrophobic IF2 is more tightly restricting water passage in and out of the protein oligomer interior, with COM distance of $1.08 \pm 0.03 \text{ nm}$.

The rotational orientation of individual helices around their principal axes appear in our simulations to be normally distributed with an approximate width of $\sigma \approx 1.5^\circ$, frequently showing a 5° deviation from the crystal structure in either direction. This is attributed to the difference in temperature and environment between crystallization and simulation, but appears to constitute relaxation and not be in any case functionally

	Solution		Membrane		CEP	
SSL48	3.0	0.5	2.1	0.2	2.9	0.3
K20N	4.1	0.4	-	-	2.3	0.2
K23SE27S	3.1	0.3	-	-	2.4	0.2
G16SG17S	2.7	0.2	-	-	-	-
SSL44	-	-	3.7	0.7	4.0	0.2
SSL47	-	-	3.3	0.3	3.7	0.1
IF1D	8.1	0.7	8.5	0.8	-	-
IF2D	5.5	0.6	2.3	0.4	4.9	1.1

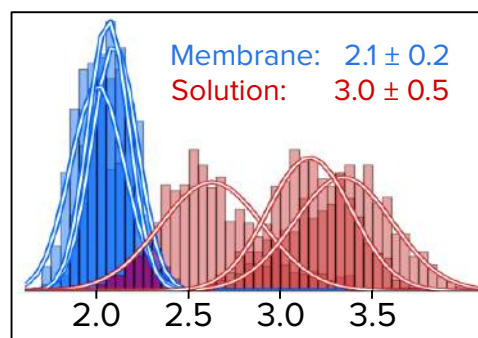


Figure 14 & Table 4: Structural stability represented by RMSD, all measurements in Å, standard deviation in bold. Illustration of the distribution of RMSD across the simulation frames for the comparison of SSL48 in solution and membrane, clearly indicating a more stable state, closer to the crystallized state in the latter environment.

important. While strong negative correlation of the rotation of adjacent helices was expected due to the tight packing and frequent contact of adjacent helices, this was not consistently observed, indicating that the width of the rotational distributions represent individual helix fluctuations restricted by residue binding to adjacent helices, rather than a global backbone correlation. The major dictating interaction that appears to determine the stability of the oligomeric assembly is therefore flexible sidechain interactions, rather than determined by the secondary structure in preferential packing.

Dimeric structures in solution show a more prominent reduction of the radius of gyration compared to hexameric simulations, associated with an apparent hydrophobic collapse-type structure deformation. This is unsurprising for IF1D which exposes much of the hydrophobic content of the protein to solvent. Rotation of helices around their principal axis is in this case much more prominent, and strongly correlated. Examining the reaction coordinate in which we could conceive dimers to inter-convert by anti-correlated rotation, this manifests itself clearly, but due to helices undergoing significant destabilization (cf. Fig. 14 and Fig. 15A) this coordinate loses its legitimacy as describing the helices as idealized cylinders, nor is interconversion ever observed or indicated to be plausible.

7.2.2 Zn ion retention

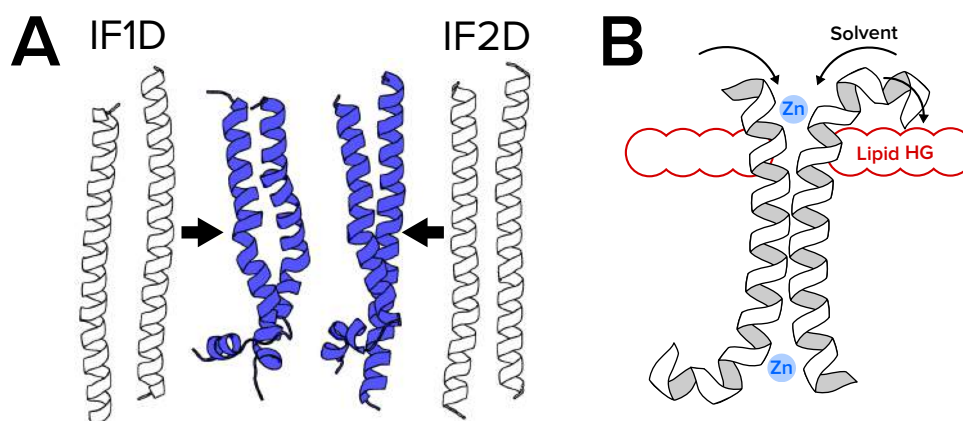


Figure 15: A) IF1/2D structure deformation in solution and membrane environments after 200ns and **B)** an illustration of the solvent exposure of the ion binding site in IF1D upon insertion and lipid HG interaction of the peptide termini.

Zn²⁺ ion binding appears stable in solution even in IF1D. Interestingly, IF1D inserted into a lipid bilayer is not able to retain Zn²⁺ ions, due to the interaction of peptide terminal ends with lipid HGs, separating and increasing exposure of Zn²⁺ ion-binding sites to solvent (cf. Fig. 15B). Negative HGs of the POPG also causes a locally elevated Na⁺ ion concentration, constituting a competitive element for the negative sidechains which bind Zn²⁺. Simulations show Zn²⁺ ions losing interaction with none, one or both of IF1D monomers on the simulated timescales, rendering IF1D unstable when inserted. Considering its only moderate

stability in solution, IF1D is not likely a physiologically relevant oligomeric state. IF2D is however as stable upon insertion as when incorporated into the hexamer, and consequently the more likely oligomeric precursor.

7.2.3 Mutants

The single mutation K20N is investigated for its likely evolutionary origin (cf. fig 16A1 and 5) and structural significance (cf. Fig. 16A1). Additionally we construct a double mutant K23SE27S to investigate the role of this charge-pair as a possible steric restriction and permeation barrier in the channel center, as observed in the crystal structure hexameric assembly. The basis for selection of these two mutants is illustrated in Fig. 16. Both mutants investigated perturb the mid-sequence interactions which stabilize monomer interfaces via

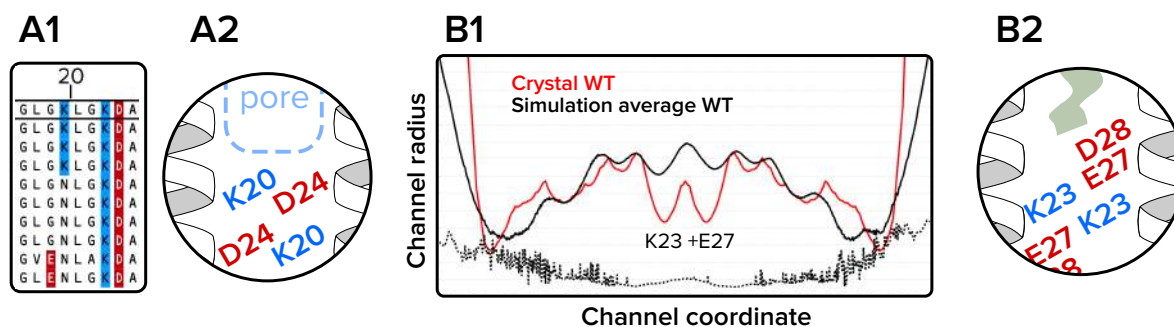


Figure 16: Bioinformatical basis for investigation of K20N mutant (A1) which stabilizes IF1 (A2), and similarly the structural basis for the double mutation of the charge-pair K23+E27 to serine (B1) which in crystal structure appears significantly blocking the channel, as well as stabilizing IF2 (B2).

charge-zipper pairs, implying the significance of all mutated residues as structural stabilizers, corroborated by an elevated RMSD (cf. Table 4) in solution. The RMSD is reduced in a membrane, as in SSL48 (cf. section 6.2.1). The disruption of the binding pattern in both mutants produces far reaching effects in the structure, exemplified by the organization of the internally lining sidechains (cf. Fig. 17C). The K20N mutant does no longer form a charge-pair with D24, which leads to increased flexibility of adjacent sidechains as far away as residues D45, and similarly for the mutated charge pair K23-E27. These central, charged residues are in the WT observed to form a highly temporally conserved binding pattern (cf. Fig. 16), affording the hexamer a rigidity that is evidently decreased in the examined mutants.

7.2.4 Truncations

SSL48 is *in-vivo* proteolytically cleaved of its C-terminal leucine [17], and indications from collaborators are of concomitant increase in antimicrobial potency. Structurally we hypothesize that this is due to removal of the helical offset (c.f Fig. 6B) which closes the canonical (linear) permeation path, and we thus construct simulations of SSL47 hexamers based on the SSL48 crystal structure to investigate the potentially increased resulting conductance. The Zn^{2+} ion binding observed is localized to residues H38-D42 [21], and by evidence of the restricting role of D45 (cf. Fig. 17C) along the canonical path a further C-terminal truncation SSL44 might have a similar but more drastic effect on conductance. The elevated RMSD observed in the simulation of truncations is likely due to the loss of helix termini association, increasing the flexibility of the immediately preceding sequence of residues. In SSL44 this could destabilize Zn^{2+} retention, but apart from a slight rise in RMSD no such effect is observed.

7.3 Channel interior

Examination of the crystal structure interior using MOLE [39] reveals a possible steric restriction by residue Lys-23 to a channel radius of 2.2 Å in the central region of the channel interior (cf. Fig. 16B1). However, upon examination of the dynamic behavior of SSL48 in a membrane, this restriction is dominated by Glu-27

at $3.5 \pm 0.5 \text{ \AA}$. Interestingly, under a TMV the mean radius in this region widens even further to a value of $4.3 \pm 0.5 \text{ \AA}$ (cf. Fig. 17), but now again dominated by Lys-23. We interpret this as Glu-27 acting evasively under a TMV rather than invasively under no TMV, affording this observation little causal value for ion permeation. The crystal structure should however be given limited weight due to its inherently different environment of origin. Other residues show a limited or insignificant effect on channel radius restriction during absence and presence of a TMV.

The mutant K23SE27S was rationally designed to examine the effect of the channel radius on conductance,

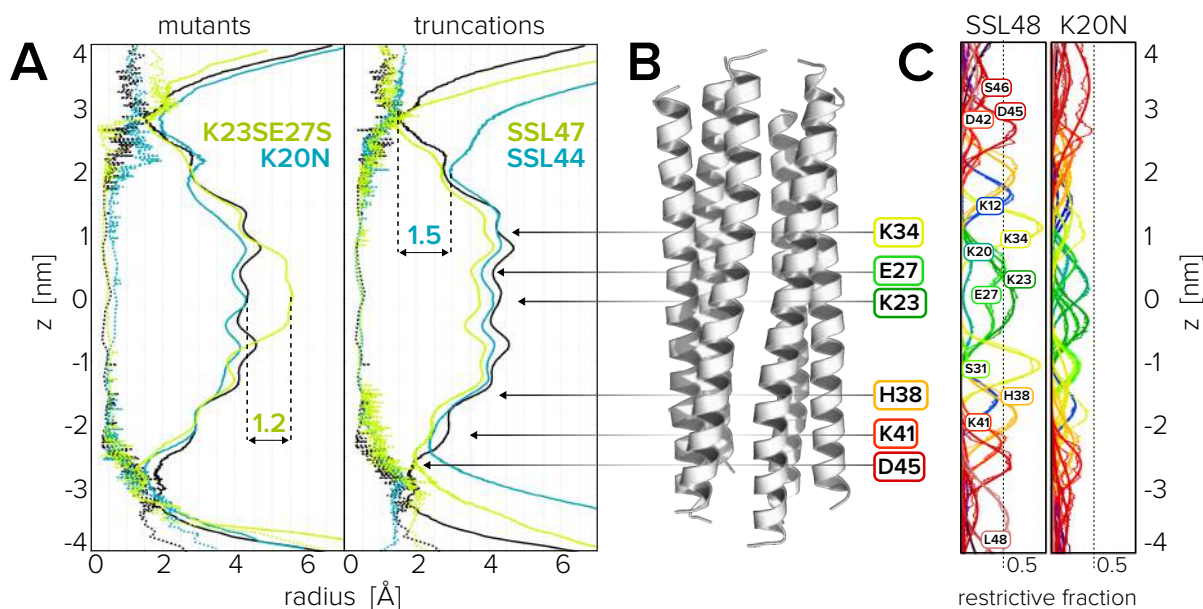


Figure 17: Channel radii determined for structures over $3 \times 100 \text{ ns}$ in a 3:1 POPE:POPG bilayer under TMV. Dashed lines denote standard deviation. Error in the mean is omitted due to insignificant magnitude. Fractional contribution per residue to channel restriction is also displayed as a function of channel coordinate, peak fitting according to double Gaussian restricted to $\mu_1 = -\mu_2$, illustrating the loss of temporal organization of the channel interior upon mutation of a single 'charge-zipper'-associated residue K20.

and has an insignificant effect on in spite of an increased central region radius to $5.5 \pm 0.5 \text{ \AA}$, now the widest part of the channel interior (cf. Fig. 17A). It does succeed to despecify the restrictive residues throughout the channel interior, indicating that residues Lys-23 and Glu-27 establish a structural role beyond their mutual interaction.

The mutant K20N has a negligible effect of channel radius, but similarly perturbs the pattern of restricting residues, indicating its similar structural role in not only channel rigidity but interior residue interaction specificity. Importantly we note that although the radius remains at a similar value to the WT, the disruption of the binding pattern (cf. Fig. 17C) coincides with an increased Na^+ ion permeability in both mutations, indicating a preference of Na^+ ions to permeate by intermediate binding to the negative residue sidechains that were previously occupied by lysine sidechains.

Truncation sequences appear to retain a rigid interior, as expected following an unperturbed charge-zipper. The insignificant increase in conductance of SSL47 compared to WT simulations at similar circumstances [21] does not aid the explanation reported increase in antibacterial activity, whereas CEP simulations of SSL44 show a clearly higher conductive capacity (cf. Fig. 20), likely due to opening of the canonical permeation pathway as illustrated by the channel radius profile (cf. Fig. 17). We are however not able to verify this with a quantified metric at present, leaving the possibility open that the absence of Na^+ ions aggregating at the C-termini changes the electrostatic environment to in this way enable a higher conductance through the WT permeation pathway.

7.4 Ion translocation pathway

While both ion species desolvate during permeation, Na^+ ions do so more readily, depleting about half of their first solvation shell. There is also desolvation of Na^+ ions at the membrane interface following an elevated ion concentration and ion immobilization, both due to negative lipid HG's $\sim 3\text{nm}$ from the membrane midplane (cf. Fig. 18). The permeation of Cl^- ions through the SSL48 channel was observed to proceed by entry and

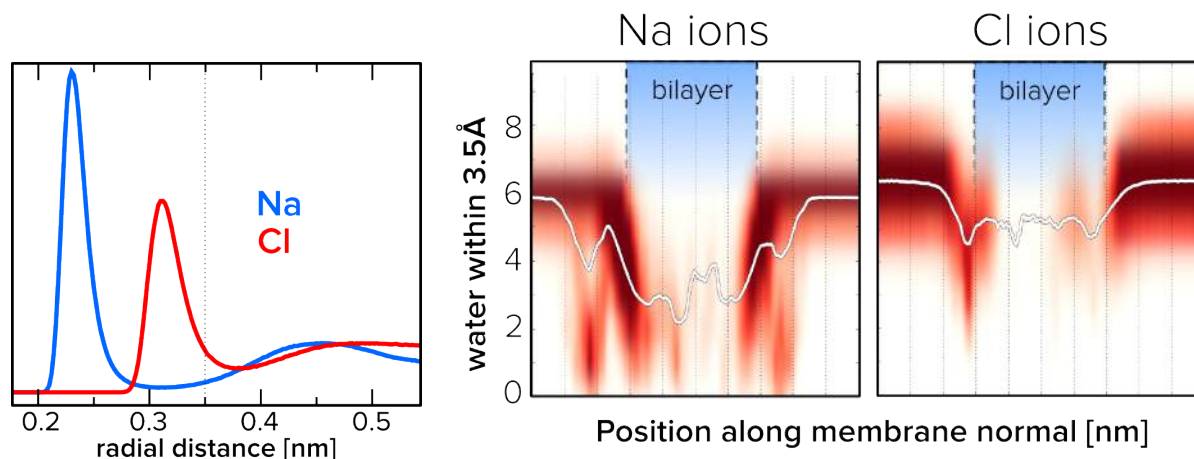


Figure 18: Radial distribution of water oxygen atoms around ions during WT CEP simulation (A) and the number of average number of water oxygens within a 3.5\AA of ions, resolved along membrane normal axis (B). The latter also displays the underlying 2D histogram.

exit through openings in IF1 (cf. Fig. 19) [21], which become exposed to solvent by the acquired 30° tilt of the principal axis of the oligomer. This pathway displayed a high selectivity for Cl^- ions over Na^+ , which permeate to a lesser extent and then via discontinuous movement along the protein exterior by side-chain 'hopping'. This decreases their mobility compared to the largely solvated Cl^- ions, which we speculate is in part what enables the higher rate of permeation of the latter due to the lack of available sidechains for Na^+ ions to interfacially bind.

Na^+ ions are observed to regularly interact with SSL48 residues across its sequence, but is dominant at the 4 C-terminal residues, and the central channel exterior (cf. Fig. 19). Notably, K20 appears to have an above 1/hexamer occupancy, but this is likely due to occasional proximity to D24 which interacts with Na^+ ions. Overall Na^+ ions display wholly more side-chain prone interactions compared to Cl^- ions, penetrating into the hydrophobic membrane region in a desolvated state even in the absence of a TMV. Extending simulations and enforcing a TMV proves to establish an increased equilibrium occupancy. Ultimately our simulations show that occupancy of positive ions at negative residue sidechains is the equilibrium state even deep into the hydrophobic region of the membrane.

Only four residues show a time-averaged Cl^- ion occupancy over half an ion per hexamer, in decreasing order K12, H38, K34 and K41 (cf. Fig.19). The latter three are separated by single helical turns, and all four are situated immediately inside the entry/exit pore. Direct contact of Cl^- ions with these residues appears frequent and transient in view of the still high degree of solvation in this region (cf. Fig. 18), reflecting their role in supplying a favorable electrostatic environment rather than opportunities for direct Cl^- ion binding. This likely contributes to Cl^- ion capture into the channel, and agrees well with an observed sequestering of Cl^- ion density to these regions and exclusion from the channel midpoint. Despite being largely solvated in the channel, Cl^- ions are then not completely free to diffuse through it due to the electrostatic environment of the channel interior. Positive sidechains in the central channel region show no prominent Cl^- interactions, filling solely structural roles as a charge-zipper to negative sidechain residues. The positive residues K6 and K13 show frequent but highly transient contacts with Cl^- ions but are situated immediately outside the entry/exit pore. We speculate that this acts to some extent conduct Cl^- ions into the pore region or increase the attempt frequency for pore entry. The K13 sidechain spans almost the entire pore, plausibly acting as a

discriminator against Na^+ ion entry into the channel interior, Na^+ ions being exceedingly rare to occur inside the channel. However the localization of K6 and K13 both coincide with the lipid HG region of the bilayer, and so is equally likely to constitute functionally important interactions with lipid HGs.

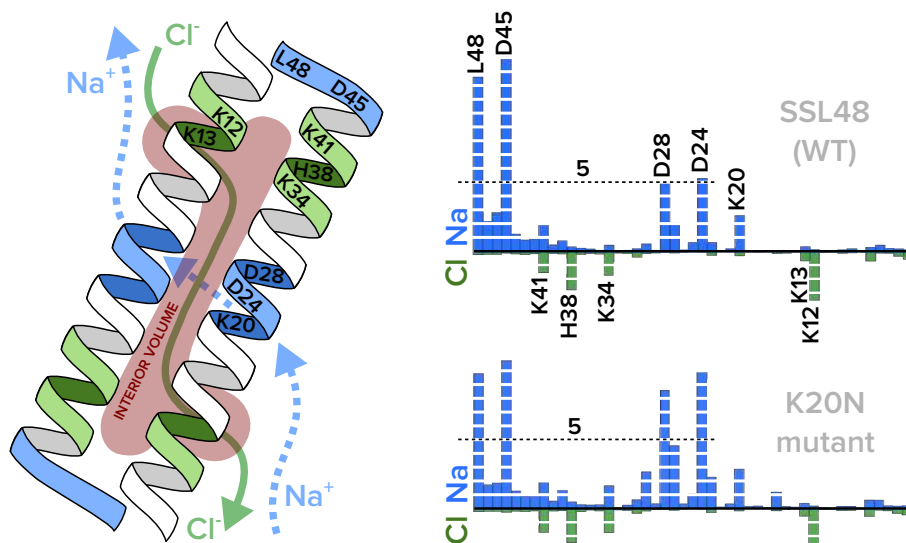


Figure 19: The observed permeation behavior for Na^+ and Cl^- ions are apparently separate and independent, the latter interior to the protein and solvated, the former exterior and partially desolvated. Average ion interactions are plotted for each residue in the 48aa sequence, and the K20N mutant increases mid-sequence flexibility to increase the local interactions with Na^+ ions, which increase the Na^+ ion permeation rate and decreases the proteins ion selectivity.

7.5 Ion conductance

7.5.1 Voltage-dependence

The determination of channel conductance proceeds via assumptions of ohmic behavior, which is in fact not conclusively verified with the present data, being insufficient to establish a confident linear dependence, as can be seen in Fig. 20. While there is little reason to expect non-ohmic behavior, the partitioning of simulation time to assess momentary correlation between ion current and voltage reduces support for this causal link, voltage not being sufficient to determine ion current in CEP simulations on timescales shorter than ~ 50 - 100 ns. Assuming underlying ohmic behavior an average conductance over longer timescales in high voltage simula-

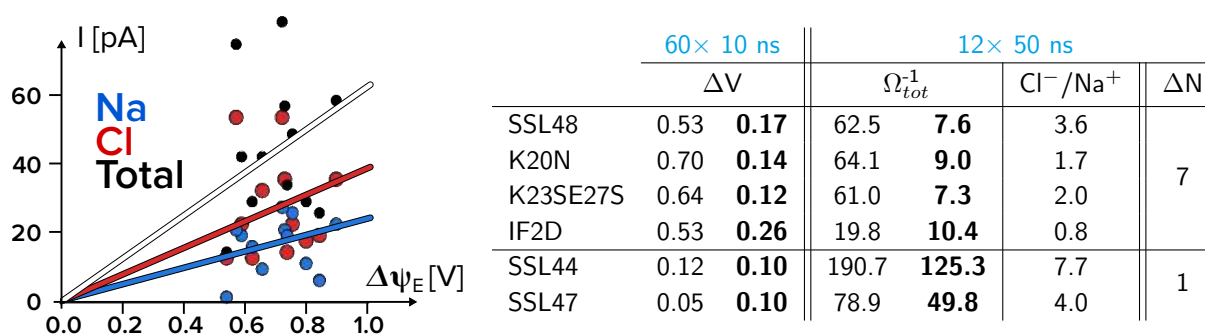


Figure 20 & Table 5: Current vs. voltage plot for K20N mutant to exemplify general voltage-dependence, which is detailed in the adjacent table for all investigated systems. Bold values are i) standard deviations for voltage, ii) standard error for conductance. ΔN indicates the number of ions of imbalance that were maintained in simulations. For single ions imbalance ($\Delta N = 1$) simulations an ion concentration of 1M was used, otherwise 0.15M. The large uncertainty in conductances for truncated structures is attributed to the lower voltage and consequent sensitivity to fluctuations at an elevated ion concentration. Truncations however display consistently higher conductive *capacity* compared to WT 1.0M/ 0.1V simulations (108 ± 11 pS).

tions is still valid, judging from the relatively low (15%) uncertainty estimation of the overall conductances

(cf. table in Fig. 20). Either fluctuations are due to the ion current rather than causing it, or not so long-lived as to cause an observable change in the momentary ion current. The latter is reasonable, given that voltage varies on timescales much shorter than we require to get even a moderate confidence interval for the average conductance. Reasonably then, to fully judge the validity of a linear current-voltage dependence in a CEP setup, the established average voltage needs to be varied, calling for additional simulations. While we cannot afford time to examine this further in the present work, we shall proceed with knowledge that average properties over entire 100ns ranges are those which have legitimate statistical support.

7.5.2 Poissonian modeling

The data for all simulations is collected in Table 6. The additive property of rates for separate ion species appears to be fulfilled for WT SSL48, permeation of Cl^- constituting a *continuous* Poissonian process, and to a large but lesser extent for Na^+ ions. We may at this point only speculate as to why this is, but the selectivity for Cl^- ions reduces the statistical certainty of the deviation. Moreover the Na^+ ions permeate by way of intermediate positions with high affinity for negative residue sidechains, which it makes it sensitive to the protonation state assignment. This introduces further and more prominent uncertainty for the permeation of Na^+ ions, which we cannot conclusively state a consistent permeation behavior for. Nonetheless, in so much as that the conduction process of ions can be described as Poissonian, the conductance of either ion species *is* thus independent of the other (i.e. they show no correlation). This is interesting since SSL48 enables both Na^+ and Cl^- to cross a membrane.

The K23SE27S mutant retains independent permeation paths, while the mutant K20 interestingly does not, indicating the correlation of an IF1-associated Na^+ path on Cl^- permeation. This is in line with Cl^- entry exit via pores in IF1, rationalizing this induced correlation. This further implicates IF1 central residues as associated with Cl^- passage, presumably due to electrostatic interactions since there are no prominent direct contacts observed.

The IF2D structure shows conductive behavior that can be quantifiably examined as well, while IF1D shows no activity that yields a meaningful analysis. In IF2D we see a wholly different behavior from the hexamer, transient pores being formed by the exposed charged residues attracting lipid HG into the hydrophobic region. The dichotomous open/close and non-selective nature of pore-formation results in disagreement of the rate and the average frequency as well as complete breakdown of selectivity. Since pores remain on timescales that are large compared to the inverse of the conduction rate, this effectively pauses the Poissonian process, and consequently the average behavior is not descriptive of the conductive process. Essentially, a time-averaged conductance, while physiologically relevant, does not describe its *capacity* for conductance, and moreover cannot resolve multiple processes.

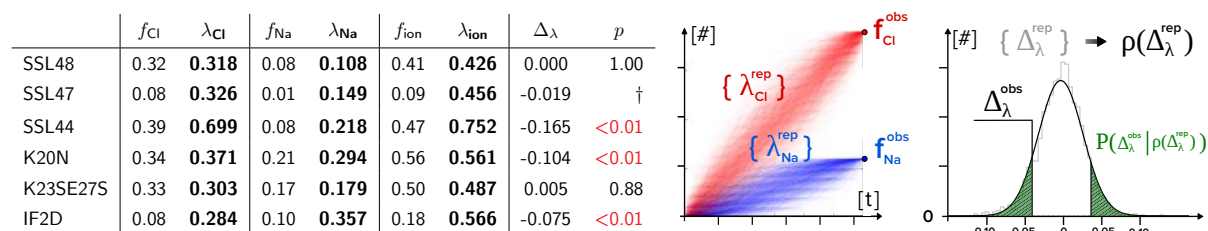


Figure 21 & Table 6: Comparison of average conduction rates to those determined using a Poissonian model. The p -values are based on a replicated probability distribution $\rho(\Delta\lambda^{\text{rep}})$, and states the likelihood of the observed $\Delta\lambda$ given the observed number of events and assuming ion permeation occurs according to independent Poisson processes. († = inconclusive due to low statistics of permeation)

7.5.3 Water flux and conductance

Simulations constructed to assess osmotic contribution to water flux showed no statistically significant net water flow using concentration differences lower than 0.3M, validating the negligible influence of an osmotic

effect on conducted simulations of SSL48-derived structures. However a simulation using aquaporin-1 under a concentration difference of 1.0M, yielded a flux counter to the concentration gradient, consistent with an osmotic effect. The flux in this simulation (2 tetrameric AQP1 complexes) was found to be 1.0 ns^{-1} , and the volumetric flux per AQP1 monomer was determined as $p_f = 2 \cdot 10^{-13} \text{ cm}^3 \text{ s}^{-1}$ per protein monomer, one order of magnitude above the experimentally determined value [42]. Examining this apparent osmotic effect, forwards and backwards currents (j_{\uparrow} and j_{\downarrow}) are expected to be proportional to the effective concentration of water in either compartment. A conductance value of 1.0 ns^{-1} over a 100ns trajectory, and the approximate water molarity of 55M and 54M in compartments with NaCl concentrations of 0M and 1M respectively, yields (for the simulation as a whole) coupled equations for the directional currents in a concentration-dependent model (indexed $o=observed$, $e=expected$):

$$\begin{cases} j_{\uparrow}^o - j_{\downarrow}^o = 100 \\ j_{\uparrow}^e / j_{\downarrow}^e = 55/54 \end{cases} \quad \text{if } (j_{\uparrow}^e, j_{\downarrow}^e) = (j_{\uparrow}^o, j_{\downarrow}^o) \Rightarrow \begin{cases} j_{\uparrow}^e = 5500 \\ j_{\downarrow}^e = 5400 \end{cases} \quad (6)$$

The 5ps interval of simulation frame output is able to identify most of the events, but unexpectedly an exclusion zone of 2.5 \AA according to that described in section 5.5.4 (cf. Fig. 12), finds the directional permeation numbers to be $j_{\uparrow}^o = 2818$ and $j_{\downarrow}^o = 2731$. This equates to a net average current of 0.9 ns^{-1} , reasonably consistent with the net count at 1.0 ns^{-1} , but *is* in disagreement with the predicted absolute permeation rates in either direction, and thus cannot validate the rate of directional water flow as is expected from an osmotic driving force. Although no confident conclusion in the matter of inherent dynamics or functional knowledge of AQP1, we may conclusively claim that no indication of intra-compartment water flux that will significantly influence that caused by ion flux in simulations of SSL48-derived peptides exist, and importantly that the system we refer to as evidence for this would in deed be able to show such an effect it were present, even at higher osmotic pressures.

The values of net water transport by ion permeation established by Eq.(4) appear inconclusive. In part this might be due to the equal weight given to either ion species, in spite of their established separate permeation paths (c.f section 6.5.2) and dissimilar degree of solvation while in the hydrophobic region of the membrane. Re-weighting Eq. (4) to account for a solvation of 2:1 for Cl ion current over Na as indicated by Fig. 18 does not improve noticeably on the variability between simulation trajectories. Further consideration of this weighting would conceivably improve the understanding of secondary water transport caused by ion permeation in this channel structure, but we have not been able to establish a meaningful interpretation as of yet.

7.6 Oligomerization and insertion pathway

The considered mutations have confidently modified function, and we turn to evaluate the functionality of these changes with respect to alteration of the structure stability and oligomerization kinetics. Solution simulations of dimeric subunits indicate a mutual instability of both dimeric subunits. In a membrane-inserted state, however, there is a significantly lower RMSD and more preserved interactions to argue the hydrophobic IF2D dimer subunit as the only physiologically plausible lower oligomeric state. The stable tertiary structure in this subunit conceivably further stabilizes Zn^{2+} ion binding across IF1 in the hexamer by keeping the termini from splitting, thus not enabling the competitive exclusion of Zn by solvent access to the binding site. This supports the notion of the IF2D subunit as a requisite for the formation of IF1, and consequently formation earlier in the oligomerization pathway. Additionally IF2D is the only of the two dimeric structures that can sustain a membrane-permeabilizing effect in simulations with a TMV, possibly constituting another active conformation of SSL48, albeit as we observe in simulation a less effective such in terms of ion gradient decoupling capacity. Although we cannot argue the insertion to occur at the monomeric, dimeric or hexameric stage, we are confident in claiming that the dimerization into IF2D occurs after contact with a membrane, indicating that the selective activity of SSL48 is associated with either favorable insertion or aggregation of IF2D subunits into higher oligomers, most importantly the hexameric state.

7.7 Conclusions

Returning to the questions outlined, we can now give credible response to them in turn:

- **Is there a structural basis for the observed anion selectivity, and is it significantly preserved across taxa? - YES**

There is sufficient evidence to support the notion of independent permeation of Na^+ and Cl^- ions by poissonian modeling. Supporting this further are the mutants studied, both of which affect the permeation of Na^+ ions to approach the conductance Cl^- ions. Expanding the central oligomer cavity does not significantly increase conductance but correlates with loss of rigidity. Therefore we conclude that the selective exclusion of Na^+ ions displayed by the WT SSL48 *in-silico* is attributable to the high rigidity of the oligomer caused by charge-matching of residue sidechains in the central membrane region. Perturbing this complementarity introduces a lesser selectivity, although not completely consistent with the concentration of the respective ions species in solution, signifying the still more expedient translocation of Cl^- ions along its permeation pathway compared to Na^+ ions. Truncated sequences an increase in anion selectivity, arguing the activation of a secondary Cl^- ion permeation path as predicted, as well as the plausibly similar ion gradient decoupling effect of shorter dermcidin-derived peptides.

- **Can an insertion pathway of dermcidin explain its selectivity for bacteria? - NO EVIDENCE**

There is strong evidence to argue IF2D as a stable intermediate for further oligomerization, IF1D being unstable in an inserted state. In addition IF2D shows a membrane-permeabilizing effect in partially negative HG lipid bilayers, and transient non-selective ion conductance under a TMV. Together these facts point towards a possibly functional oligomerization intermediate in an inserted state, which then aggregates towards a full hexameric state via Zn ion coordination. The conditions under which the hexameric crystal structure was obtained objects this notion, however the crystal structure displays a degree of helicity that far exceeds that of solution-NMR [36] or CD-spectroscopy [20]. So while there are conflicting reports of secondary structure to base any final oligomeric state on, these do not argue against the hexameric as an active conformation. There is however no immediate evidence to explain bacterial specificity by stability considerations of the examined structures and environments. While we can hypothesize an inserted and stable IF2D subunit to be a necessary step in the oligomeric assembly, we have not established a stabilizing factor exclusive to bacterial membranes.

- **Is there a lipid-interaction basis for a localization selectivity of dermcidin to bacterial membranes? - NO EVIDENCE**

The role of lipids in the permeation behavior appears wholly passive, although there are interactions with dimeric structures which actively perturb Zn ion stability and thus any further oligomerization. While the question of lipid specificity can to some extent be addressed using the structures examined, the fundamental variable is clearly the lipid species used. While preliminary results indicate large differences depending on lipid components as well as incorporation of cholesterol, these are not statistically verified or structurally examined in full, and we refrain from speculation.

- **Can we, using knowledge gained from answering the previous questions, enhance or modify channel function using rational design mutation(s) of the peptide sequence? - YES**

We do not, as of yet, have any verified predictive knowledge of how changes to the structure affect the function of behavior of the hexameric structure. Given this, we cannot claim to be able to modify or improve its function with any confidence. We do argue that the detailed explanation of the function of SSL48 tells us enough to intelligently reason on how changes to sequence will affect the protein dynamics, and in this sense we claim to have modified function without decreasing its apparent efficiency as an antibiotic. Further the constructed truncations show a significant increase in conductive capacity. Ultimately, experimental verification will have to provide the final verdict to this question.

8 Discussion

8.1 Results in view of previous work

The dependence of the function of dermcidin-derived peptides on Zn has been observed [19] and is credibly explained by the structure and herein observed mode of action of it as an ion gradient decoupling oligomeric assembly. Antimicrobial activity has been established for C-terminal truncations occurring *in-vivo* down to SSL45 [19], which agrees with the preservation of the residues involved in Zn^{2+} ion binding as indicated by the crystal structure. Based on this notion we constructed SSL44, which although not present in native sweat samples, indeed also appears to retain function. N-terminal truncations show insignificant activity in experimental studies [19], further corroborating the charge-zipper of the crystal structure and the coordination of Zn^{2+} into oligomers. While the voltages achieved in CEP simulations are high compared to the reported breakdown voltage of about 0.2V [43] [44] of most biomembranes, the simulated membrane is robust to this high voltage over the timescales probed. Simulated membranes are thus implausibly stable, however the principal observable using this setup is the conductance, a property which we increase sampling of at a higher voltages. Moreover, the simulated timescales and size limitations of the patches, as well as the presence of a voltage-decoupling membrane protein can be legitimately claimed to significantly alter the expected membrane stability. Conclusions on the structural role of lipids in ion permeation are consequently less confident, but reasonable in view of the relatively short total simulated time.

To maintain comparability of residue-ion interactions between simulations, a high voltage and low ion concentration (0.15M/0.6V) was maintained over mutation- and dimer-simulations. The alternate low voltage / high ion concentration (1.0M/ 0.1V) scheme was implemented for truncation simulations in order to provide potential experimental comparison to conductance values [21]. While the latter is realistically favorable, the former offers a system wherein ion-sidechain interactions are not flooded, yet achieves sufficiently increased sampling.

The permeation of Cl^- ions at a higher degree of hydration compared to Na^+ ions is consistent with observed effects during electroporation [43], in which Na^+ ions are able to permeate a pore before it is fully formed, while Cl^- ions require a more substantial water bridge. This has been attributed to the difference in VdW-interactions of the respective ion species with lipid headgroups, which drastically differentiates the membrane-surface mobilities of the two ions.

Concerning the partially conducting state of the IF2D, pore formation becomes a plausible event in atomistic simulations under applied TMVs of more than 0.4-0.7V [45], even in the absence of any membrane permeabilizing molecule [43]. Therefore the activity of IF2D in CEP should perhaps be interpreted as decreasing the cost of pore formation and stabilization of existing pores. Negative mechanical pressure needed to exceed -200 bar in order to induce pore formation in another computational study [46], but could feasibly affect the properties of existing pores at lower pressures than this. Simulations however show no indication of such negative pressures, nor an elevated A_L . The calculated A_L of 0.60 nm^2 in IF2D simulations is in agreement with reference values reported for similar lipids [47], and the lipid diffusion rate of $1.9 \times 10^{-8} \text{cm}^2 \text{s}^{-1}$ is an order of magnitude lower than that reported for pure lipid membranes [48], and thus reasonable in view of the presence of protein in the presently simulated membranes.

The assignment of SSL48 as an aAMP relies on default protonation states, which are reasonable to assume only in solution. The protonation state in hydrophobic environments is highly uncertain but indications have been given from experimental studies that a charged state is largely unaffected by a hydrophobic environment [49] [50]. Specifically these studies single out arginine sidechains to always retain a charged state in hydrophobic pockets, of which SSL48 has none. Unless lysine is structurally essential over arginine (something we see no immediate indication of) the absence of arginine is evolutionary unlikely and thus significant. Assignment of lysine sidechains as unambiguously charged might therefore be wrong, or obfuscating a dynamic property of lysine residues. This points out that the simultaneous designation of SSL48 as native to a membrane, and the aAMP antimicrobials, is equally based on assumptions of default protonation states.

8.2 Alternate interpretation

The designation of the hexameric assembly as natively membrane-inserted is strengthened by coarse-grain simulations performed by Dr. Chen Song (unpublished), wherein the lipid phase is allowed to auto-assemble in the presence of the hexameric assembly, resulting in a favorable orientation in the normal (however tilted) orientation as opposed to parallel.

Further considering the sequence, the charge pattern of the AMP domain of the DCD gene is strikingly complementary in an anti-parallel matching, in agreement with the crystallized structure. This charge pattern has been observed as a 'charge zipper' even before the oligomeric structure was published [51], but the interpretation was then that the helix folded back onto itself between K23 and D24. Given the extraordinary length of SSL48 as a TM helix domain, this argument is appealing, but ultimately not more favorable than the inter-molecular matching of pairs of helices which the crystal structure shows. An interesting observation however, given the reported antimicrobial effect of shorter sequences like SSL25 [20], which would conform to a more conventional TM helix length yet lack this charge-zipper altogether. While the crystallographic assignment of a hexameric oligomer itself is unambiguous, there is nothing that immediately objects to any 2-fold multimeric state based on the minimum dimeric unit. While reports are of a single oligomeric species in solution [23], the aggregation of dimeric units into larger complexes is likely to result in several such states. While we have not endeavored to examine tetra- or octameric states, feasibly one might be able to, although a tetramer would likely have too narrow an internal cavity to effectively conduct ions which permeate predominantly solvated.

The working hypothesis of ion gradient decoupling is a sufficient but not necessary requirement for bacterial lethality. The ability of all but one of the studied SSL48-derived structures to sustain a water-column across the bilayer is sufficient to decouple the pH-gradient which bacteria frequently establish across their cytosolic membranes. The lethality of SSL48 by means of enabling proton diffusion has not been studied, but is to be considered significant since even full water permeation appears even more expedient than ion permeation.

8.3 Outlook

8.3.1 Additional simulation

By further simulation there are a number of ways to extend the conclusions of oligomerization. Simulation of the inserted hexameric conformation lacking either an IF1D or IF2D unit, could serve to validate the stabilization of Zn^{2+} ion binding by the addition of a hydrophobic helix interface, as is implied by the results of IF1D simulations in the present work.

Given the simulations already completed, the most strategic extension would be to complement those into thermodynamic cycles, which could serve to deconvolute the influence of ion concentration, mutations and TMV on conductance. The further simulations investigating the effect of different lipid membranes and incorporation of cholesterol into the membrane are an instrumental part in this view, and the natural starting point for building knowledge on the conclusions of the present work. Simulations are currently examining conductances of SSL48 in CEP setups in DAPC, DSPC, DPPC, and DMPC bilayers, as well as DMPC bilayers containing cholesterol, which seek to quantify the change in conductance between bacterial and non-bacterial membranes, to explain the specificity of SSL48-derived peptides for bacterial membranes. These are conducted in a high concentration / low voltage setup, making them inherently sensitive to trajectory fluctuations, and therefore far too low on statistics at present to make any speculation as for their effect.

A prospect briefly mentioned but not considered quantitatively in the present work is the possible pH decoupling effect of SSL48 and its derivatives by the establishment of a full water bridge across a biological membrane. We simply assume that the water column, which is sufficient to establish a full solvation shell for Cl^- ions during permeation, is able to accommodate proton hopping and constitute an additional lethality for bacterial

cells which commonly utilize pH-gradients for energy synthesis. However there is evidence of strong orientation of water molecules in the interior of the protein, due to the strong accumulation of Na^+ ions at the negative lipid HGs as well as the C-termini of the protein monomers which tie together at the end of the channel structure. While a TMV is likely sufficient to overcome this it might still affect proton mobility. The lesser water column observed in the permeabilizing dimer structure IF2D is also feasibly decoupling a pH gradient although ion permeation is limited. Both of these scenarios are open for testing by specialized simulation setups which require proton diffusion to be modeled. Reasonably, however, its implementation into the CEP setup is straightforward.

8.3.2 Experimental extension

Initial examination of the effect of alternate protonation state assignment of SSL48 sidechains showed a breakdown in ion selectivity, at the time unattributable to any specific causal relationship. We are now able to plausibly argue a similar de-specification of sidechain charge-zipper interaction and the following destabilization as observed for mutants. Observing high selectivity *in-vivo* would thus correspond to correctly chosen protonation states based on the stabilizing complementarity that maintains the ion selectivity. There are no such experimental observations yet, but the increased stability of the default protonation states chosen as opposed to the destabilized structure constitutes (an albeit very weak) indication of preference. The destabilization of the considered mutants, which seem implausible to affect Zn^{2+} binding could constitute a verification of the oligomeric state assignment and protonation states chosen.

The experimental verification of this and in extension the retained oligomeric state and channel structure of truncations SSL44 and SSL47 by for instance native gel electrophoresis and electrophysiology is the most direct confirmation of the results in the present work. We have been able to establish experimental observables in conductance and selectivity for ion species, as well as water permeability values that is experimentally verifiable, and so this is in principle straightforward to endeavor. An interesting approach to perhaps increase the potency of SSL48-derived peptides artificially is to link together several monomers with a flexible linker, the hypothesis being that this would increase the rate of oligomerization. An extension of such an approach would be to assay two or more distinct linkers with different preferential insertion into a lipid bilayer. Considering one linker with a low (L) insertion barrier and one with a high (H), the relative orientation and insertion of different combinations of such linkers could elucidate whether oligomerization occurs prior to insertion, as is illustrated in Fig. 22. A consequence of these different linkers is the conceivable verification of the results by the examination of oriented insertion, as all inserted structures are oriented (cf. Fig. 22).

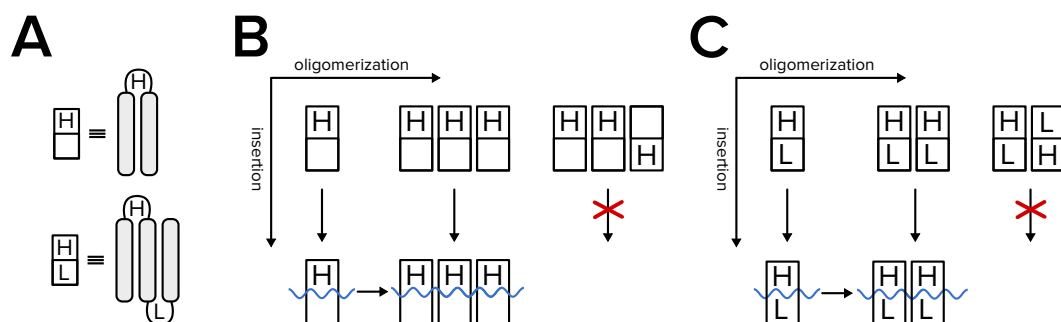


Figure 22: Using linkers to connect monomers one could feasibly increase the rate of oligomerization or minimum inhibitory concentration. By extension using distinct linkers with a low (L in Fig) and high (H in Fig) barrier of insertion, we here conceive two linked units (A) which could differentiate between a pre- and post-inserted oligomerization into the hexameric form. Compared to a variant with exclusively L-linkers the two variants (B) and (C) would show a decreased activity if oligomerization occurs prior to insertion.

8.4 Ethical considerations

The widespread use of antibiotics was initially stated as causing the increased emergence of antibiotic-resistant strains of bacteria, and thus necessitating the development of novel antibiotics. The implementation of any novel such drug would similarly cause directed evolution towards further resistance, which while not unexpected, is unpredictable. It is said that 'necessity is the mother of invention', and this aptly describes the threat of artificially increasing the rate of evolution in bacteria, in that while there is no immediate need to develop new ways for *bacteria to target eukaryotes*, the progress of this is slow. *If* we in fact are able to create a novel antibiotic, the eventual resistance (which itself might not be exceptionally difficult for bacteria to attain) might realize a strain which is wholly more potent or virulent than its predecessor, and now resistant to multiple antibiotics. This is the intricate problem of evolution and its relation to the use of antibiotics. Nature has no universal antibiotic, doubtless for this precise reason; such a thing would direct evolution towards resistance at a rate that would render it less effective or completely ineffective that much quicker. It appears through this reasoning that mankind must do that which they are least apt to; establish a level of equilibrium in which the desired effect is balanced to the impact on the surroundings. There is little room in this notion for the introduction of novel antibiotics, but the careful study of antibiotics will hopefully afford insights into their evolutionary effect on bacterial resistance development prior to their implementation, as this is likely to affect their efficacy and potent lifetime.

9 Acknowledgments

I owe the most profound thanks to my advisor at the Max-Planck Institute in Göttingen, Prof. Bert de Groot, for the opportunity to join his group for the period of my masters project, as well as the freedom to take this project where my curiosity lead me. Throughout he has always been willing to discuss, guide and teach, and there is little more I could have hoped for.

As for the opportunity to join the group for Biomolecular Dynamics, and indeed the entire department of Theoretical and Computational Biophysics in Göttingen, its value resides in its members. For me, to be able to discuss on a daily basis every aspect of research and my scientific methods, listen in on diverse branches of biochemical and biophysical methodologies, and learn from the wealth of knowledge that resides in this moderately sized German city, was a staggeringly enriching experience. I owe them all the sincerest of thanks, and in deed a generous portion of fare-well desert which somehow got lost in the wealth of things to arrange when my time at the department came to an end.

Special thanks are due to Carsten Kutzner, David Köpfer, Shreyas Kaptan and Vytautas Gapsys, without whose individual expertise in methods utilized in this thesis, it would have been all the much poorer. And to Eveline 'Evi' Heinemann; secretary extraordinaire, landlord, bringer of reimbursements, coffee and all other of those things without which scientists would surely perish, I doubt that any of the members of the department are any less willing than I to pledge myself eternally grateful. In similar fashion I would not have gotten far, nor would most of those involved in computational methods, without the perpetual vigilance of sysadmins, in my case Martin Fechner and Ansgar Esztermann.

References

- [1] M. Zasloff. Antimicrobial peptides of multicellular organisms. *Nature*, 415(6870):389–395, 2002.
- [2] B. Schitteck, R. Hipfel, B. Sauer, J. Bauer, H. Kalbacher, S. Stevanovic, M. Schirle, K. Schroeder, N. Blin, F. Meier, G. Rassner, and C. Garbe. Dermcidin: a novel human antibiotic peptide secreted by sweat glands. *Nature Immunology*, 2(12):1133–1137, 2001.
- [3] Nagendra N. Mishra, Arnold S. Bayer, Truc T. Tran, Yousif Shamoo, Eugenia Mileykovskaya, William Dowhan, Ziqiang Guan, and Cesar A. Arias. Daptomycin resistance in enterococci is associated with distinct alterations of cell membrane phospholipid content. *Plos One*, 7(8), 2012.
- [4] A. Peschel, M. Otto, R. W. Jack, H. Kalbacher, G. Jung, and F. Gotz. Inactivation of the *dlt* operon in staphylococcus aureus confers sensitivity to defensins, protegrins, and other antimicrobial peptides. *Journal of Biological Chemistry*, 274(13):8405–8410, 1999.
- [5] Ron Saar-Dover, Arkadi Bitler, Ravit Nezer, Liraz Shmuel-Galia, Arnaud Firon, Eyal Shimoni, Patrick Trieu-Cuot, and Yechiel Shai. D-alanylation of lipoteichoic acids confers resistance to cationic peptides in group b streptococcus by increasing the cell wall density. *Plos Pathogens*, 8(9), 2012.
- [6] H. X. Zhou, G. N. Rivas, and A. P. Minton. *Macromolecular crowding and confinement: Biochemical, biophysical, and potential physiological consequences*, volume 37 of *Annual Review of Biophysics*, pages 375–397. Annual Reviews, Palo Alto, 2008.
- [7] Raquel F. Epand, Paul B. Savage, and Richard M. Epand. Bacterial lipid composition and the antimicrobial efficacy of cationic steroid compounds (ceragenins). *Biochimica Et Biophysica Acta-Biomembranes*, 1768(10):2500–2509, 2007.
- [8] A. B. Hooper and A. A. Dispirito. In bacteria which grow on simple reductants, generation of a proton gradient involves extracytoplasmic oxidation of substrate. *Microbiological Reviews*, 49(2):140–157, 1985.
- [9] T. J. Cunningham, H. Y. Jing, Y. Wang, and L. Hodge. Calreticulin binding and other biological activities of survival peptide γ -p30 including effects of systemic treatment of rats. *Experimental Neurology*, 163(2):457–468, 2000.
- [10] G. D. Stewart, R. J. E. Skipworth, J. A. Ross, K. C. H. Fearon, and V. E. Baracos. The dermcidin gene in cancer: role in cachexia, carcinogenesis and tumour cell survival. *Current Opinion in Clinical Nutrition and Metabolic Care*, 11(3):208–213, 2008.
- [11] Hyun Ho Jung, Sung-Tae Yang, Ji-Yeong Sim, Seungkyu Lee, Ju Yeon Lee, Ha Hyung Kim, Song Yub Shin, and Jae Il Kim. Analysis of the solution structure of the human antibiotic peptide dermcidin and its interaction with phospholipid vesicles. *Bmb Reports*, 43(5):362–368, 2010.
- [12] Min Li, Kevin Rigby, Yuping Lai, Vinod Nair, Andreas Peschel, Birgit Schitteck, and Michael Otto. Staphylococcus aureus mutant screen reveals interaction of the human antimicrobial peptide dermcidin with membrane phospholipids. *Antimicrobial Agents and Chemotherapy*, 53(10):4200–4210, 2009.
- [13] Shigeru Matsuoka, Ji Mao, and Masayuki Inoue. Effects of the phosphatidylglycerol head group on the binding of short dermcidin-derived peptides to the phospholipid membrane surface. *Tetrahedron Letters*, 53(9):1078–1081, 2012.
- [14] I. Senyuerek, G. Doering, H. Kalbacher, M. Deeg, A. Peschel, C. Wolz, and B. Schitteck. Resistance to dermcidin-derived peptides is independent of bacterial protease activity. *International Journal of Antimicrobial Agents*, 34(1):86–90, 2009.

- [15] Ilknur Senyuerek, Maren Paulmann, Tobias Sinnberg, Hubert Kalbacher, Martin Deeg, Thomas Gutschmann, Marina Hermes, Thomas Kohler, Fritz Goetz, Christiane Wolz, Andreas Peschel, and Birgit Schitteck. Dermcidin-derived peptides show a different mode of action than the cathelicidin II-37 against staphylococcus aureus. *Antimicrobial Agents and Chemotherapy*, 53(6):2499–2509, 2009.
- [16] D. Baechle, T. Flad, A. Cansier, H. Steffen, C. Garbe, B. Schitteck, and H. Kalbacher. Postsecretory processing of dcd-1l by cathepsin d in human eccrine sweat. *Journal of Investigative Dermatology*, 125(3):A9–A9, 2005.
- [17] D. Baechle, T. Flad, A. Cansier, H. Steffen, B. Schitteck, J. Tolson, T. Herrmann, H. Dihazi, A. Beck, G. A. Mueller, M. Mueller, S. Stevanovic, C. Garbe, C. A. Mueller, and H. Kalbacher. Cathepsin d is present in human eccrine sweat and involved in the postsecretory processing of the antimicrobial peptide dcd-1l. *Journal of Biological Chemistry*, 281(9):5406–5415, 2006.
- [18] Birgit Schitteck, Maren Paulmann, Ilknur Senyuerek, and Heiko Steffen. The role of antimicrobial peptides in human skin and in skin infectious diseases. *Infectious Disorders - Drug Targets*, 8(3):135–143, 2008.
- [19] Birgit Schitteck. The multiple facets of dermcidin in cell survival and host defense. *Journal of Innate Immunity*, 4(4):349–360, 2012.
- [20] Maren Paulmann, Thomas Arnold, Dirk Linke, Suat Oezdirekcan, Annika Kopp, Thomas Gutschmann, Hubert Kalbacher, Ines Wanke, Verena J. Schuenemann, Michael Habeck, Jochen Buerck, Anne S. Ulrich, and Birgit Schitteck. Structure-activity analysis of the dermcidin-derived peptide dcd-1l, an anionic antimicrobial peptide present in human sweat. *Journal of Biological Chemistry*, 287(11):8434–8443, 2012.
- [21] Chen Song, Conrad Weichbrodt, Evgeniy S. Salnikov, Marek Dynowski, Björn O. Forsberg, Burkhard Bechinger, Claudia Steinem, Bert L. de Groot, Ulrich Zachariae, and Kornelius Zeth. Crystal structure and functional mechanism of a human antimicrobial membrane channel. *Proceedings of the National Academy of Sciences*, 110(12):4586–4591, 2013.
- [22] M.A. Larkin, G. Blackshields, N.P. Brown, R. Chenna, P.A. McGettigan, H. McWilliam, F. Valentin, I.M. Wallace, A. Wilm, R. Lopez, J.D. Thompson, T.J. Gibson, and D.G. Higgins. Clustal w and clustal x version 2.0. *Bioinformatics*, 23(21):2947–2948, 2007.
- [23] I. Cipakova, J. Gasperik, and E. Hostinova. Expression and purification of human antimicrobial peptide, dermcidin, in escherichia coli. *Protein Expression and Purification*, 45(2):269–274, 2006.
- [24] J. L. Popot and D. M. Engelman. Membrane-protein folding and oligomerization - the 2-stage model. *Biochemistry*, 29(17):4031–4037, 1990.
- [25] A. Peschel and H. G. Sahl. The co-evolution of host cationic antimicrobial peptides and microbial resistance. *Nature Reviews Microbiology*, 4(7):529–536, 2006.
- [26] K. Burke. Perspective on density functional theory. *Journal of Chemical Physics*, 136(15), 2012.
- [27] Jeffery B. Klauda, Richard M. Venable, J. Alfredo Freites, Joseph W. O'Connor, Douglas J. Tobias, Carlos Mondragon-Ramirez, Igor Vorobyov, Jr. MacKerell, Alexander D., and Richard W. Pastor. Update of the charmm all-atom additive force field for lipids: Validation on six lipid types. *Journal of Physical Chemistry B*, 114(23):7830–7843, 2010.
- [28] Rüdiger Goetz and Reinhard Lipowsky. Computer simulations of bilayer membranes: Self-assembly and interfacial tension. *The Journal of Chemical Physics*, 108(17):7397–7409, 1998.
- [29] G. van Meer, D. R. Voelker, and G. W. Feigenson. Membrane lipids: where they are and how they behave. *Nature Reviews Molecular Cell Biology*, 9(2):112–124, 2008.

- [30] D. P. Tieleman, J. L. MacCallum, W. L. Ash, C. Kandt, Z. T. Xu, and L. Monticelli. Membrane protein simulations with a united-atom lipid and all-atom protein model: lipid-protein interactions, side chain transfer free energies and model proteins. *Journal of Physics-Condensed Matter*, 18(28):S1221–S1234, 2006.
- [31] W. Im, M. Feig, and C. L. Brooks. An implicit membrane generalized born theory for the study of structure, stability, and interactions of membrane proteins. *Biophysical Journal*, 85(5):2900–2918, 2003.
- [32] S. Villinger, R. Briones, K. Giller, U. Zachariae, A. Lange, B. L. de Groot, C. Griesinger, S. Becker, and M. Zweckstetter. Functional dynamics in the voltage-dependent anion channel. *Proceedings of the National Academy of Sciences of the United States of America*, 107(52):22546–22551, 2010.
- [33] Bert L de Groot and Helmut Grubmüller. The dynamics and energetics of water permeation and proton exclusion in aquaporins. *Current Opinion in Structural Biology*, 15(2):176 – 183, 2005.
- [34] D. A. Kopfer, U. Hahn, I. Ohmert, G. Vriend, O. Pongs, B. L. de Groot, and U. Zachariae. A molecular switch driving inactivation in the cardiac k⁺ channel herg. *Plos One*, 7(7):11, 2012.
- [35] Sander Pronk, Szilard Pall, Roland Schulz, Per Larsson, Par Bjelkmar, Rossen Apostolov, Michael R. Shirts, Jeremy C. Smith, Peter M. Kasson, David van der Spoel, Berk Hess, and Erik Lindahl. Gromacs 4.5: a high-throughput and highly parallel open source molecular simulation toolkit. *Bioinformatics*, 29(7):845–854, 2013.
- [36] Sunhwan Jo, Taehoon Kim, Vidyashankara G. Iyer, and Wonpil Im. Charmm-gui: A web-based graphical user interface for charmm. *Journal of Computational Chemistry*, 29(11):1859–1865, 2008.
- [37] M. G. Wolf, M. Hoefling, C. Aponte-Santamaria, H. Grubmuller, and G. Groenhof. g_membed: Efficient insertion of a membrane protein into an equilibrated lipid bilayer with minimal perturbation. *Journal of Computational Chemistry*, 31(11):2169–2174, 2010.
- [38] Carsten Kutzner, Helmut Grubmueller, Bert L. de Groot, and Ulrich Zachariae. Computational electrophysiology: The molecular dynamics of ion channel permeation and selectivity in atomistic detail. *Biophysical Journal*, 101(4):809–817, 2011.
- [39] O. S. Smart, J. M. Goodfellow, and B. A. Wallace. The pore dimensions of gramicidin-a. *Biophysical Journal*, 65(6):2455–2460, 1993.
- [40] O. S. Smart, J. G. Neduvilil, X. Wang, B. A. Wallace, and M. S. P. Sansom. Hole: A program for the analysis of the pore dimensions of ion channel structural models. *Journal of Molecular Graphics and Modelling*, 14(6):354–, 1996.
- [41] Yingting Liu and Fangqiang Zhu. Collective diffusion model for ion conduction through microscopic channels. *Biophysical Journal*, 104(2):368–376, 2013.
- [42] F. Q. Zhu, E. Tajkhorshid, and K. Schulten. Theory and simulation of water permeation in aquaporin-1. *Biophysical Journal*, 86(1):50–57, 2004.
- [43] Andrey A. Gurtovenko and Ilpo Vattulainen. Ion leakage through transient water pores in protein-free lipid membranes driven by transmembrane ionic charge imbalance. *Biophysical Journal*, 92(6):1878–1890, 2007.
- [44] R. A. Bockmann and S. W. I. Siu. Electric field effects on membranes: Gramicidin a as a test ground. *Journal of Stuctural Biology*, 157(3):545–56, 2007.
- [45] D. Peter Tieleman. The molecular basis of electroporation. *BMC Biochemistry*, 5:10–Article No.: 10, 2004.

- [46] D. P. Tieleman, B. Hess, and M. S. P. Sansom. Analysis and evaluation of channel models: Simulations of alamethicin. *Biophysical Journal*, 83(5):2393–2407, 2002.
- [47] Krzysztof Murzyn, Tomasz Róg, and Marta Pasenkiewicz-Gierula. Phosphatidylethanolamine-phosphatidylglycerol bilayer as a model of the inner bacterial membrane. *Biophysical Journal*, 88(2):1091–1103, 2005.
- [48] A. Filippov, G. Oradd, and G. Lindblom. The effect of cholesterol on the lateral diffusion of phospholipids in oriented bilayers. *Biophysical Journal*, 84(5):3079–3086, 2003.
- [49] Michael J. Harms, Jamie L. Schlessman, Gloria R. Sue, and Bertrand Garcia-Moreno E. Arginine residues at internal positions in a protein are always charged. *Proceedings of the National Academy of Sciences of the United States of America*, 108(47):18954–18959, 2011.
- [50] Daniel G. Isom, Carlos A. Castaneda, Brian R. Cannon, and Bertrand E. Garcia-Moreno. Large shifts in $pK(a)$ values of lysine residues buried inside a protein. *Proceedings of the National Academy of Sciences of the United States of America*, 108(13):5260–5265, 2011.
- [51] Torsten H. Walther, Christina Gottselig, Stephan L. Grage, Moritz Wolf, Attilio V. Vargiu, Marco J. Klein, Stefanie Vollmer, Sebastian Prock, Mareike Hartmann, Sergiy Afonin, Eva Stockwald, Hartmut Heinzmann, Olga V. Nolandt, Wolfgang Wenzel, Paolo Ruggerone, and Anne S. Ulrich. Folding and self-assembly of the tata translocation pore based on a charge zipper mechanism. *Cell*, 152(1-2):316–326, 2013.
- [52] H. M. Eriksson, P. Wessman, C. R. Ge, K. Edwards, and A. Wieslander. Massive formation of intracellular membrane vesicles in escherichia coli by a monotopic membrane-bound lipid glycosyltransferase. *Journal of Biological Chemistry*, 284(49):33904–33914, 2009.